NPS-OC-91-004

NAVAL POSTGRADUATE SCHOOL
Monterey, California

THESIS

CHARACTERIZATION OF THE CLOCK IN A NEW INEXPENSIVE GPS RECEIVER: THE MAGNAVOX MX 4200

by

Manuel Pardo

September, 1991

Thesis Advisor: James R. Clynch

Approved for public release; distribution unlimited

Prepared for:
Naval Postgraduate School
Monterey, California 93943-5000

NAVAL POSTGRADUATE SCHOOL
Monterey, California

Rear Admiral R. W. West, Jr.
Superintendent

H. Shull
Provost

This thesis is prepared in conjunction with research sponsored and funded by the Naval Postgraduate School (NPS).

Reproduction of all or part of this report is authorized.

UNCLASSIFIED

SECURITY CLASSIFICATION OF THIS PAGE

REPORT DOCUMENTATION PAGE

Form Approved OMB No 0704-0188

1a REPORT SECURITY CLASSIFICATION UNCLASSIFIED	1b RESTRICTIVE MARKINGS
2a SECURITY CLASSIFICATION AUTHORITY	3 DISTRIBUTION / AVAILABILITY OF REPORT Approved for public release; distribution is unlimited
2b. DECLASSIFICATION / DOWNGRADING SCHEDULE	
4. PERFORMING ORGANIZATION REPORT NUMBER(S)	5 MONITORING ORGANIZATION REPORT NUMBER(S)
6a. NAME OF PERFORMING ORGANIZATION Departament of Oceanography Naval Postgraduate School 6b OFFICE SYMBOL (*If applicable*) OC	7a. NAME OF MONITORING ORGANIZATION Naval Postgraduate School
6c. ADDRESS (*City, State, and ZIP Code*) Monterey, CA 93943 - 5000	7b ADDRESS (*City, State, and ZIP Code*) Monterey, CA 93943 - 5000
8a. NAME OF FUNDING / SPONSORING ORGANIZATION 8b OFFICE SYMBOL (*If applicable*)	9 PROCUREMENT INSTRUMENT IDENTIFICATION NUMBER OM&N
8c. ADDRESS (*City, State, and ZIP Code*)	10 SOURCE OF FUNDING NUMBERS PROGRAM ELEMENT NO / PROJECT NO / TASK NO / WORK UNIT ACCESSION NO

11 TITLE (*Include Security Classification*)
Characterization of the Clock in a New Inexpensive GPS Receiver: the Magnavox MX 4200

12. PERSONAL AUTHOR(S)
Manuel Pardo, Lieutenant Commander, Spanish Navy

13a TYPE OF REPORT	13b TIME COVERED	14 DATE OF REPORT (*Year, Month, Day*)	15 PAGE COUNT
Master's Thesis	FROM 09.89 TO 09.91	1991, September 26th	135

16 SUPPLEMENTARY NOTATION
The views expressed in this thesis are those of the author and do not reflect the official policy or position of the DoD or the U.S. Government.

17 COSATI CODES			18 SUBJECT TERMS (*Continue on reverse if necessary and identify by block number*)
FIELD	GROUP	SUB-GROUP	GPS, Oscillator Stability

19 ABSTRACT (*Continue on reverse if necessary and identify by block number*)

A new generation of inexpensive GPS receivers is emerging, which utilize temperature compensated crystal oscillators (TCXO) as clocks. The MX 4200 has been chosen as a representative sample of this emerging technology receiver. A detailed discussion on the receiver architecture and its implications in the measurement process is given. Experiments on the sensitivity of its clock to environmental effects, as well as the duration of the transient regime are described. One limitation to the use of these receivers in geodetic applications is the stability of its clock. The noise in the receiver clock has been characterized by the Allan variance for sampling intervals up to 4000 seconds. The implication of the noise level for short time intervals on the applicability of the receiver to high precision work is examined.

20 DISTRIBUTION / AVAILABILITY OF ABSTRACT	21 ABSTRACT SECURITY CLASSIFICATION
☒ UNCLASSIFIED/UNLIMITED ☐ SAME AS RPT ☐ DTIC USERS	Unclassified
22a NAME OF RESPONSIBLE INDIVIDUAL James R. Clynch	22b TELEPHONE (*Include Area Code*) (408) 646-3268 22c OFFICE SYMBOL OC-CL

DD Form 1473, JUN 86 *Previous editions are obsolete.*

S/N 0102-LF-014-6603

SECURITY CLASSIFICATION OF THIS PAGE

UNCLASSIFIED

Approved for public release; distribution is unlimited

CHRACTERIZATION OF THE CLOCK IN A NEW INEXPENSIVE GPS RECEIVER: THE MAGNAVOX MX4200

by

Manuel Pardo
Lieutenant Commander, Spanish Navy
B.S., Spanish Naval Academy, 1975

Submitted in partial fulfillment of the
requirements for the degrees of

MASTER OF SCIENCE IN HYDROGRAPHIC SCIENCE
and
MASTER OF SCIENCE IN PHYSICAL OCEANOGRAPHY

from the

NAVAL POSTGRADUATE SCHOOL
September 1991

ABSTRACT

A new generation of inexpensive GPS receivers is emerging, which utilize temperature compensated crystal oscillators (TCXO) as clocks. The MX4200 has been chosen as a representative sample of this emerging technology receiver. A detailed discussion on the receiver architecture and its implications in the measurement process is given. Experiments on the sensitivity of its clock to environmental effects, as well as the duration of the transient regime are described. One limitation to the use of these receivers in geodetic applications is the stability of its clock. The noise in the receiver clock has been characterized by the Allan variance for sampling intervals up to 4000 seconds. The implication of the noise levels for short time intervals on the applicability of the receiver to high precision work is examined.

C.1

TABLE OF CONTENTS

I. INTRODUCTION: THE SUBJECT OF THE RESEARCH 1

A. BACKGROUND 1

B. OBJECTIVE 2

C. RELATED WORK 3

II. AN OVERVIEW ON THE GLOBAL POSITIONING SYSTEM . . . 4

A. THE GPS CONCEPT 4

B. THE SIGNAL 5

1. Carrier 6

2. Code 8

3. Data 10

C. SYSTEM SEGMENTS 10

1. Control segment 11

2. Space segment 12

3. User segment 12

D. BIASES AND ERRORS IN THE MEASUREMENT 13

1. Biases due to the satellite 14

a. Bias in the SV clock 14

b. Bias in the SV position 14

2. Biases due to the propagation medium 15

a. Ionospheric delays 15

b. Tropospheric delays: 18

3. Biases and errors due to the receiver . . . 18
a. Receiver clock 19
b. Carrier phase ambiguity 19
c. Electronics, processing and computational noise 20
4. Observation errors 21
a. Multipath 21
b. Antenna phase center 21
E. SELECTIVE AVAILABILITY AND LEVELS OF ACCURACY . 22
F. DIFFERENTIAL POSITIONING 24

III. THE MAGNAVOX 4200 RECEIVER 26
A. GENERAL CHARACTERISTICS 26
B. INTERFACES 28
1. Control port 28
2. Raw data port 29
3. Equipment port 29
4. RTCM port 29
C. NAVIGATION MODES 30
D. TIME RECOVERY 31
E. THE MEASUREMENT PROCESS; TRACKING LOOPS 32
1. Tracking loops 32
2. Navigator 35
F. SOFTWARE AND FIRMWARE 36

IV. THE RAW DATA MESSAGE AND THE COMPUTATION OF THE MEASURABLES 38
A. THE MX4200 RAW DATA MESSAGE 38
1. Raw measurement data record, types 1 and 2 . 39
2. Solution record, type 8 40
3. Time recovery record, type 969 41
B. COMPUTATION OF THE MEASURABLES 42
C. RAW VERSUS REPORTED MEASUREMENTS 48
1. Three different time frames 49
2. Raw measurements computation 52

V. CHARACTERISTICS OF THE RECEIVER CLOCK 55
A. DETERMINISTIC EFFECTS PRESENT IN THE MEASUREMENT. 55
1. External to the clock 55
2. Internal to the clock 56
B. THE CLOCK MODEL 57
1. Data logging 58
2. Data interface 59
3. Input interface 59
4. Main algorithm 60
a. Raw data input 61
b. Receiver clock correction 62
c. OMC computation 63
d. Computation of the deterministic model . 65
e. Statistics and edition of data 67

5. Outputs 68
C. LONG TERM DETERMINISTIC EFFECTS 70
1. Transient regimes 70
2. Temperature effects 73

VI. CHARACTERIZATION OF THE CLOCK NOISE 79
A. MEASURING THE FREQUENCY STABILITY IN THE TIME DOMAIN 80
1. The Allan variance 82
2. Confidence intervals 83
B. STOCHASTIC PROCESSES IN AN OSCILLATOR 87
C. CHARACTERIZATION OF THE NOISE IN THE MX4200 RECEIVER CLOCK 90
1. Analysis tools 91
a. Program MXALLV 91
b. Program MERGE 92
c. Program MXFXRS 92
d. Program CONFIN 93
2. Short term analysis 94
3. High frequency systematic effects 99
a. Pseudorange noise 99
b. Ephemeris changes 99
c. Temporary loss of lock and cycle slips . 105
d. Selective Availability activation . . . 106
4. Long term analysis 106

VII. CONCLUSIONS 112

LIST OF REFERENCES 115

APPENDIX A. AUTHOR'S SOFTWARE 117

APPENDIX B. ARL SOFTWARE 119

APPENDIX C. DR. CLYNCH'S SOFTWARE 120

APPENDIX D. OMLS ADJUSTMENT 121

INITIAL DISTRIBUTION LIST 124

I. INTRODUCTION: THE SUBJECT OF THE RESEARCH

A. BACKGROUND

Accurate real time position and velocity is an essential piece of knowledge in many fields of science and engineering. Electronic radionavigation systems (Decca, Loran, Omega, etc.) have been successfully used in the last decades. Transit doppler satellite system was the first operational spaceborne positioning system available for scientists and surveyors in the late sixties.

None of them has had as wide an application as the Global Positioning System (GPS). First conceived as a military oriented system, its impact on navigation and surveying has been remarkable. Its level of accuracy, for short periods of observation, exceeds any other available system. But its success relies on the quality of its main component: the clock.

Different kinds of clocks have been used for this purpose, mainly quartz oscillators, rubidium and cesium resonators. Among other things, clocks have been the limiting factor, both in price and size, for certain applications. Technology in this field, as well as in integrated circuitry, has improved dramatically in the last few years. Nevertheless, crystal oscillators are very sensitive to changes in temperature.

Usually, manufacturers place the oscillator inside an oven at a fairly high temperature. This imposes severe restrictions regarding power supply requirements.

The last generation of surveying receivers, small sized and with built-in power supply, was available in the late eighties. They have tracking loops that, again, require a high performance quartz oscillator. They are expensive devices, then, although capable of levels of accuracy only expected for receivers equipped with atomic clocks before.

Great improvements have occurred in the design of a different kind of receiver. A new line of products is now emerging. They have a temperature-compensated crystal oscillator, not enclosed in an oven. Both price and power requirements have dropped dramatically. They may not be suited for high level geodetic tasks; but are entirely adequate for certain surveying or oceanographic applications.

Magnavox released its last GPS receiver, model MX4200, in January 1990. It weighs less than a kilogram, costs just over $3,000 and requires less than 3.5 watts, D.C. power. Experiments on its performance seemed to be worthwile.

B. OBJECTIVE

The objective of this research is the characterization of the clock performance in the Magnavox 4200 GPS receiver. To this end, several laboratory tests were performed to obtain the receiver measurements free of as many systematic effects

as possible. An analysis of the stochastic noise was then feasible.

As usual with brand new pieces of equipment, a great deal of research had to be devoted to try to understand the receiver idiosyncrasies, which turn out to be innovative in many respects. As emerging technology, it was subject to software and firmware modifications to upgrade its performance. All the efforts have been done to update the analysis to the last available version.

C. RELATED WORK

Clynch and Coco [Ref. 1] have investigated the short term phase noise in several clocks, from GPS measurements, to determine the limits of reconstruction of the number of whole cycles lost when phase lock is lost and regained. Colquitt and Anderle [Ref. 2] described the results of a simulation of the effects of the frequency stability, for various clocks, on the Doppler Transit measurements.

II. AN OVERVIEW ON THE GLOBAL POSITIONING SYSTEM

A general background on the GPS system is introduced here to give the reader a better understanding of later explanations. Most of it should be credited to Wells [Ref. 3].

A. THE GPS CONCEPT

The GPS is based on two elementary principles:

- Given the position of a satellite, it is possible to compute the satellite-receiver distance by measuring the time it takes for a signal sent by the satellite to get to the receiver.
- Given the frequency of a signal, it is possible to compute the radial component of the relative velocity by measuring the Doppler shift in the incoming signal.

This will provide, then, two independent measurements per space vehicle (SV). If three SV's are being observed, it is possible to solve for three spatial coordinates and three components of the velocity vector.

Actually, this is true if no error exists in the receiver clock. It may be fairly stable, but its measurements are scaled by the speed of light, which is a huge number. That is why both offset and drift of the receiver clock are computed as a part of the navigation solution. This is achieved by observing either four SV's, or only three, with an added constraint: the antenna elevation, which is sometimes fairly

well known. In both cases a deterministic solution can be obtained:

- Three SV's, range and Doppler shift each, are enough to solve for x, y, τ, $\dot{x}$, $\dot{y}$, $\dot{\tau}$.
- Four SV's, range and Doppler shift each, provide data to solve for x, y, z, τ, $\dot{x}$, $\dot{y}$, $\dot{z}$, $\dot{\tau}$.

If more than four satellites are available, redundant observations can be made. It leads to a better estimate, via a least squares solution.

The solution is usually implemented through a Kalman filter. Current measurements update a solution that accounts for its recent history. This allows for continuous solution in case a satellite is temporarily lost or if changes in the available constellation occur. In addition, this filters out a great deal of the noise in the current measurements.

B. THE SIGNAL

Three independent pieces of information are then needed to achieve the measurement:

- A reference signal to compare with the incoming Doppler shifted signal.
- Something to recognize when the signal left the SV.
- The position and dynamics of the SV at that precise epoch.

All this information is embedded in the signal the SV sends: it consists of a carrier wave of a known frequency, which is modulated by 'code' and message. The code is a repeating trend of two level states in a precise pattern, one

for each satellite. It begins at a certain, known epoch in the SV clock. The message is a set of digitally coded pieces of information regarding the SV position and status, among others.

Then the incoming signal can be expressed as:

$$S(t) = C(t)\ D(t)\ \exp(-i2\pi(f-f_d)t) \qquad (1)$$

where $C(t)$ represents the code, $D(t)$ the data and $f-f_d$ is the carrier nominal frequency, shifted by a Doppler frequency of f_d.

The way in which the carrier is modulated by code and message is not pertinent to the present discussion. But all the timing processes, as well as the signal generation, are driven by the main oscillator in the SV. Its nominal frequency, f_0, is 10.23 Mhz. Different scale factors, always integers, provide all the frequencies and time tagging used in the whole process. Thus, an error detected in any of them leads to a precise knowledge of the error in the main oscillator, and in turn, in any of the frequency and time tagging parameters.

An overview of all three follows:

1. Carrier

Two frequencies are transmitted by the SV:

- L1 at 1575.42 Mhz (154 f_0)
- L2 at 1227.60 Mhz (120 f_0)

The reasons for this choice are discussed in Spilker [Ref. 4:p. 37]. Ionospheric effects are minimum over this range of frequencies, among those available in the radionavigation bands. At the same time, they are far enough from each other so that dual frequency measurements can be accurately done, as discussed later.

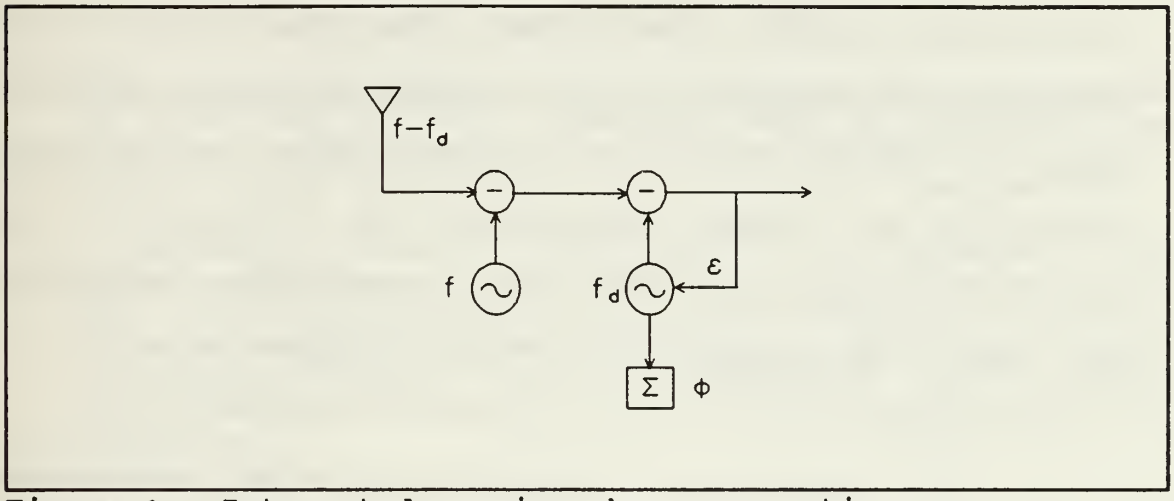

Figure 1.- Integrated carrier phase generation

The Doppler measurement is obtained by first removing the carrier frequency from the incoming signal (Figure 1). Then a Doppler tracking loop follows. A modeled Doppler frequency is generated by the tracking loop oscillator, and subtracted from the remaining signal. The oscillator frequency is continuously corrected by the error signal after the Doppler frequency removal. This modeled frequency is then the Doppler frequency measurement. This is how much the frequency of the incoming signal is offset from the nominal carrier frequency, due to the dynamics of both satellite and receiver.

If Doppler cycles are counted since tracking was locked, a quantity called 'integrated carrier phase' is obtained. This quantity, times the carrier wavelength, is called phase derived range. It is a measurement of the range to the satellite, biased by the range at the time when tracking was locked on. This quantity has a deep impact in ranging for precise positioning. Once that bias can be determined, measurements are more accurately done based on the phase. A one per cent of the total cycle can be easily determined on a phase measurement. The wavelength of the carrier is about 0.19 meters; as a consequence, the noise in this kind of measurement is in the millimeter range.

2. Code

This refers to a digitally generated pseudorandom noise (PRN). This is a long sequence of transitions, between two states, generated at a certain rate and repeating. It is known as a Gold code. When its length is very large, it approximates the true random code behavior. This is:

- It has an energy density spectrum comparable to a random, white noise. That is where its name comes from.
- The autocorrelation function shows a triangular peak, of unit height and twice the chip length wide, at no time delay. It is $1/N^2$ elsewhere, N being the number of chips integrated. Here chip refers to the interval between clock pulses.
- The cross correlation between different codes of the same nature is $1/N^2$ for any time delay. They behave as two uncorrelated white noises.

These features make the PRN code very well suited for ranging applications. It carries only two pieces of information: SV identification and transmit time. It is therefore possible to spread the signal in a wide bandwidth at very low levels of power, without compromising its reliability.

Every satellite generates two different codes:

- C/A (clear/acquisition) code, 1023 chips long, generated at 1.023 Mhz and self repeating every millisecond. The Standard Positioning Service (SPS) is implemented by means of this code. It modulates both L1 and L2 frequencies.
- P (precision) code, 267 days long. It is truncated to one week length, and repeated then. It is generated at 10.23 Mhz, so its chip length is 1/10 that of the C/A code. This allows levels of accuracy an order of magnitude better than using C/A code. The Precise Positioning Service (PPS) is implemented through this code. It modulates only the L1 frequency.

Implicit in the code is the transmit time. The code generation is driven by the main oscillator in the satellite. The oscillator cycles count is in fact the realization of the clock. Thus, each transition corresponds to a precise time in the satellite clock.

The measurement is done by means of a code tracking loop. A replica of the corresponding code is generated in the receiver. It is been delayed until maximum output from a correlator is obtained. Once this process is locked on, the code stays tracked by feeding back the corrections, due to misalignment between code and replica, to the existing delay. This delay is then the essence of the measurement, which is

requested at a given epoch time of measurement. This delay, times the speed of light, is called pseudorange.

3. Data

Generated at 50 bps chip rate, there is a data signal that takes 12.5 minutes to be completed. Within this period, information regarding the tracked satellite, termed ephemeris, is repeated every 30 seconds. The ephemeris data contains the orbital parameters of the SV. It allows the user to compute the SV position and velocity. Corrections to the received signal, due to misalignment between the SV clock and the absolute time, are contained in the ephemeris, too. Thus, data in the message allows the user to know, at the best real time accuracy level, the position of the satellite and the error in its clock. The high rate at which these data are transmitted allows the reciver the acquisition of a satellite in a fairly short time.

The rest of the information, termed almanac, is related to the whole constellation. It facilitates the searching of any other satellite. Status of the whole system is broadcast here, too, as well as many other special messages.

C. SYSTEM SEGMENTS

It is customary to divide the system in three main components: control, space and user segments.

1. Control segment

This consists of five monitoring stations around the globe, which continuously track all the satellites in view. By fitting the recently measured ranges to an orbital model, the Operation Control Center (OCS) adjusts the parameters of that orbit. That data is injected to the SV's, as a new ephemeris set, daily. These ephemeris sets are considered valid for two hours before and after their time of epoch. They give the position of the SV within 1 part per million. Almanacs are recomputed and injected to the whole constellation on a weekly basis.

Time keeping is the second major issue in the control segment. Every control station is equipped with cesium atomic clocks; even so, they differ relative to each other. Currently, five cesium clocks at the OCS serve as the master clock. They are adjusted every two days by comparison with the standard at the US Naval Observatory. Once the ground stations have an absolute time, it is possible to solve for the SV clock error. A second order polynomial model of its clock is included as a part in the ephemeris set.

It is worthwhile to say something about the GPS time system. It was set to zero at 00h 00m 00s UTC, January 6th 1980, and is based on weeks of 604800 seconds of UTC time. The time is then expressed in weeks (WN) and seconds within the week (SOW). Because of the irregular rate of rotation of the Earth, the time community corrects the deviation between UTC

and true rotation by adding/subtracting a leap second once in a while. This is not true for GPS time. That is why there is a 7 second difference between GPS and UTC times as of September 1991.

2. Space segment

This consists of the satellites themselves. As stated, the SV's broadcast the almanac and ephemeris data, in addition to generating C/A and P codes. All electronics are driven by a main atomic oscillator (they have spares, too) whose error is reported in the ephemeris.

The orbital geometry has been designed to provide 3-D continuous coverage worldwide: six orbital planes, at 55^0 inclination, with four SV's each. The orbit is almost circular and the height above the Earth's surface is about 20,000 Km. This makes the orbital period 12 hours. At such a height, about 5 hours out of 12, a satellite is above the observer's horizon.

As of September 1991, only 17 SV's are available. This, indeed, provides 2-D continuous coverage worldwide. A 3-D coverage is expected by the end of 1991.

3. User segment

This represents the user's end of the system: the receiver. A great variety of receivers have been designed, and they differ in many respects:

- Single (L1) versus dual frequency (L1 and L2).

- C/A versus C/A+P codes tracking.
- Main oscillator: quartz, rubidium, cesium and combinations.
- Single tracking channel versus multiple channels.
- Continuous tracking versus sequential and multiplexing.

All receivers have in common the existence of an error in their clocks, which has to be computed as a part in the navigation solution, regardless how small it is. The final application usually determines its performance: it is related to the desired level of accuracy, as well as other constraints in size, power requirements and price.

D. BIASES AND ERRORS IN THE MEASUREMENT

As usual in the scientific literature, a bias is an error in a measurement that can be identifiable and somehow modeled or computed. It may or may not be removed from the measurement. A true error, on the other hand, can have an identifiable source, but cannot be modeled. It properties can be estimated. Statistical variables are used to describe its effect on the measurement accuracy.

Biases and errors must be properly treated in making a GPS measurement. They can be classified into four main groups, depending on their source: due to the SV, to the propagation medium, to the receiver and observation errors.

1. Biases due to the satellite

There are two sources of error here:

a. Bias in the SV clock

A model of it is contained in the ephemeris message, so a great deal of it can be removed as a bias. This is effectively done, in software, by all the receivers. Some small errors (up to 10 m) remain.

b. Bias in the SV position

The real time solution is produced by using the orbital parameters in the broadcast ephemeris. Those parameters correspond to a projected orbit, as computed from previous range data to the OCS stations. Thus, it is based on an extrapolation technique. How well those parameters will describe the true orbit determines the size of this bias. It can be estimated about 5m, sometimes up to 10.

A smaller bias can be obtained using what is called 'precise ephemeris'. This set of orbital parameters is computed after tracking a SV for eight days. It is available for a postprocessing, and is based on an interpolation technique. Precise ephemeris provides a more accurate SV clock model, too. The Defense Mapping Agency (DMA) and the National Geodetic Survey (NGS) have their own tracking station networks. Both agencies produce precise ephemeris, but its distribution is very limited.

2. Biases due to the propagation medium

There are two sources of error here:

a. Ionospheric delays

The ionosphere is a dispersive medium for an electromagnetic wave. The ultraviolet light ionizes the molecules in the ionosphere, releasing free electrons. These electrons have the effect of changing both the phase and group velocity of the wave. For a differential element of time, dt, the local element of measured range will be

$$d\rho = c\ dt \tag{2}$$

because a velocity of c is assumed. For the same element of time, the true range is

$$dr = v\ dt \tag{3}$$

because v is the actual velocity of propagation.

The ratio between those elements is defined as the index of refraction. It is, in fact, the ratio between assumed and true velocities:

$$n = \frac{d\rho}{ds} = \frac{c}{v} \tag{4}$$

The measured range, then, will be

$$\rho = \int_0^{\rho} d\rho = \int_0^{s} n \; ds \tag{5}$$

Pseudorange is a measurement of a time delay. Thus, it is based on the propagation of the wave energy. The energy propagates at the group velocity. On the other hand, the phase of the signal travels at the phase velocity. Local group and phase indices of refraction can be expressed, as a high frequency approximation, as [Ref. 3:p. 9-2]:

$$n_g = \frac{c}{v_g} = (1 + a\frac{N}{f^2}) \tag{6}$$

$$n_p = \frac{c}{v_p} = (1 - a\frac{N}{f^2}) \tag{7}$$

where v_g, v_p are the group and phase propagation velocity and n_g, n_p group and phase indices of refraction. a is a certain constant, f the frequency and N is the ionospheric electron density (electrons/m^3).

The measured pseudorange, thus, will be

$$\rho = r + \frac{a}{f^2}\int_0^{r} N \; ds = r + a\frac{N_t}{f^2} \tag{8}$$

whereas the measured phase range is

$$\rho_\phi = r - a\frac{N_t}{f^2} \qquad (9)$$

N_t refers to integrated electron count along the path.

Estimated quantities for these variables are:

- a about 40 m^3 s^{-2}.
- N about 10^{12} m^{-3} (electrons per cubic meter).
- f about 1.5 x 10^9 Hz for the L1 carrier.

N_t has a maximum in daytime, and a minimum during the nighttime. It depends also on the elevation angle: the lower the SV, the larger the integration path through the ionosphere.

Calling $d_i = (a\ N_t)/f^2$ the ionospheric delay, the measured pseudorange is long by d_i, and the measured phase derived range is short by the same amount. Spilker [Ref. 4:p. 35] estimates that this delay, for vertical incidence, is 10 ns (3m) during nighttime and up to 50 ns (15m) in daytime. About three times these quantities occur for elevation angles of 10 degrees.

This quantity is hard to model. But it can be easily estimated from dual frequency observations by taking the difference between phase range measurements:

$$\begin{aligned}\Delta\rho_\phi = \rho_{\phi,L1} - \rho_{\phi,L2} &= -a\ N_t\ \left(\frac{1}{f_{L1}^2} - \frac{1}{f_{L2}^2}\right) \\ &= -a\ N_t\ \frac{f_{L2}^2 - f_{L1}^2}{f_{L1}^2 f_{L2}^2}\end{aligned} \qquad (10)$$

then

$$d_{i,L1} = a\frac{N_i}{f_{L1}^2} = \Delta\rho_\phi \frac{f_{L2}^2}{f_{L1}^2 - f_{L2}^2} \qquad (11)$$

b. Tropospheric delays:

The troposphere, on the other hand, is not a dispersive medium for the GPS range of frequencies. It affects both phase and range measurements in the same way. It is caused by water vapor molecules, as well as other constituents. Again, its effect is minimum at highest elevation. The dry component is about 90% of the total, and can be accurately estimated from surface atmospheric pressure measurements. The wet component is not so accurately known, because water vapor content is extremely variable with height. Its effect is much smaller, though. There are several models currently available to correct for tropospheric delays. Most of the geodetic receivers implement an algorithm to correct it, based on meteorological data input.

At sea level and vertical incidence, a rough approximation of the total tropospheric range error is 2.3 meters [Ref. 4:p. 36]. It can reach up to 20 meters at a 10 degree elevation angle.

3. Biases and errors due to the receiver

a. Receiver clock

This is the main source of errors in the measurement. The time difference between the receiver clock and GPS time produces a range error which is that difference multiplied by the speed of light. The frequency difference between the receiver clock (oscillator) and the nominal carrier frequency produces a velocity error of that difference multiplied by the carrier wavelength.

Most receivers, as stated, solve for time and frequency biases as a part of the navigation solution. These errors can be used then to correct the actual measurements by their range and velocity equivalents. How well this adjustment is achieved depends strongly on the stability of the clock, as well as on the quality of the navigation filter.

b. Carrier phase ambiguity

Most of the high performances receivers use the integrated carrier phase to improve the range measurement. The phase measurements are more accurate than the delay measurements.

Wells [Ref. 3:p. 9.14] estimates the resolution of the measurement to be about one percent of the signal wavelength. The C/A code chip length is about 300 meters, and the P code 30 meters. This leads to residual errors on the order of 3 and 0.3 meters respectively. L1 frequency, on the

other hand, has a wavelength about 20 cm, so residual errors could be about 2 mm, within a given cycle.

Integrated carrier phase is a biased measurement, though. The true range to the SV at time of lock-on is unknown: there is a certain integer number of cycles that has to be resolved. There are many different approaches to this problem. If the estimate of that bias is off by N cycles, this goes as a whole to the measurement, as an uncorrected bias. This bias amounts N times the carrier wavelength.

The same problem is found in a situation when tracking of a given satellite is lost. When tracking is resumed, an integer number of wavelengths have been lost from their count. This is known as 'cycle slips'. Different techniques have been developed to deal with this problem. If that count is not properly retrieved, the solution remains biased.

c. Electronics, processing and computational noise

There are a number of noise sources along the signal path in the receiver: antenna, pre-amp, demodulator..., all of which generate thermal noise. The resolution of the measurement is subject to hardware limitations; these lead to residual processing noise, too. Finally, there is noise in the computation process in the navigation filter: round-off residuals, etc.

Electronics and computational noise are considered to be at a much lower level than any other error here mentioned. Processing noise in the pseudorange measurement can be fairly high, though. Because of that, precise positioning is done based on phase range measurements.

4. Observation errors

Here is a group of true errors which cannot be removed, although some of them can be easily detected.

a. Multipath

Metallic surfaces act as a mirror for the incoming RF signal. What the receiver gets is a summation of direct and reflected signal. This has the effect of shifting the phase of the signal by a certain amount, depending on the relative geometry (SV-reflector-antenna). So, it shows an interference pattern as the geometry changes and is easy to recognize.

b. Antenna phase center

The radiation pattern of the antenna is not radially symmetric, as it should be. In fact, each antenna shows a different radiation pattern. So, the phase center is dependent upon the azimuth and elevation of the tracked SV.

It is very hard to know the true radiation pattern. How well it is known determines the size of the residual error. It is usually at the millimeter level.

E. SELECTIVE AVAILABILITY AND LEVELS OF ACCURACY

As mentioned above, two different services are offered by the system: Precise Positioning Service (PPS) and Standard Positioning Service (SPS). Both of them are available for military and certain civilian users. Most civilian users, however, must use the SPS. They differ in the levels of accuracy because of the size of their code chips: 300 meters for C/A (SPS), 30 meters for P code (PPS).

The system was first designed for military applications. US DoD reserves the ability to degrade both signal and message, so the quality of the solution gets worse. This is known as the 'Selective Availability' (SA) option. This might be done by broadcasting inaccurate ephemeris and by intentionally adding noise to the codes. In any event, the quality of the signals guarantees the following levels of accuracy:

- 100 meters, 2-D rms for SPS.
- 16 meters, 3-D, 1 σ, for PPS.

In an SA situation, the above accuracy of PPS requires special devices to de-crypt the degraded signals. Thus, it is useless for civilian users.

Related to the levels of accuracy is the concept of Geometrical Dilution of Precision (GDOP). It represents how much the precision in the solution is degraded due to geometrical considerations. In other words, how degraded the actual solution can be, as compared to an idealistic situation

where all tracked satellites are in an optimal spatial distribution.

The variation in the measured range to the j-th SV, due to changes in the receiver position and clock offset can be expressed as:

$$d\rho^j = \sum_{i=1}^{3} \frac{\partial \rho^j}{\partial x_i} dx_i + \frac{\partial \rho^j}{\partial \tau} d\tau \qquad (12)$$

where the partial derivatives are only determined by geometrical considerations. For measurements to n SV's, a system of equations is formed:

$$d\vec{\rho} = H \; d\vec{x} \qquad (13)$$

where each element of the design matrix H is

$$H_i^j = \frac{\partial \rho^j}{\partial x_i} \qquad (14)$$

In solving the system, the solution is found as:

$$d\vec{x} = (H^T H)^{-1} \; H^T \; d\vec{\rho} \qquad (15)$$

$(H^T H)^{-1}$ is called the covariance matrix. Its diagonal elements represent the variance in the corresponding component of the

solution. Again, only geometrical considerations affect their size.

GDOP is defined as the square root of the trace of the covariance matrix. For practical considerations, GDOP is usually 'projected' into 3 spatial coordinates and time components. Those components are termed 'Horizontal Dilution of Precision' (HDOP), 'Vertical Dilution of Precision' (VDOP), and 'Time Dilution of Precision' (TDOP). This is, taking only the first two, the third and the fourth terms of the diagonal elements of $(H^T H)^{-1}$ respectively.

GDOP can get a minimum value of one. The larger GDOP is, the larger the variance in the solution components. This is, the accuracy in the solution gets worse, just due to the relative geometry SV's-receiver.

F. DIFFERENTIAL POSITIONING

When the GPS system was first designed, it was not envisioned that there would be, in fact, several ways to overcome the limitation in the accuracy levels. It was conceived that a user would compute a real time solution, based on pseudorange measurements to determine the position.

There are many receivers that include phase measurements in the computation of the position nowadays. In addition to that, several techniques have been found to improve the solution in a post processing. Still, there is a technique that allows the common user to improve a real time solution:

differential positioning. It is based upon the assumption that most of the errors in the measurement, external to the receiver itself, are common to two receivers close enough to one another. A reference receiver can be placed on a well surveyed point. By comparing its solution with the true position, corrections either to measurements, or to coordinates, can be computed. They are then sent, real time, to the second receiver, which automatically corrects its own solution. This is a very powerful technique, of common use in the surveyor's community. It is being used for navigation purposes, too.

Differential techniques are used too in testing receivers. If the position of two receivers is known, the difference between simultaneous measurements eliminates most of the biases and errors that are external to the receivers. The distance between receivers has to be small enough to assume that ionospheric and tropospheric delays are the same for both receivers. Those differences provide an estimate of the receiver performance.

III. THE MAGNAVOX 4200 RECEIVER

A. GENERAL CHARACTERISTICS

The MX 4200 has been designed for navigation purposes, although its use for precise positioning is the object of intense research [Ref. 5]. It is a single frequency receiver, restricted to SPS users. It can continuously track the C/A code and L1 frequency of up to six satellites. The choice of satellites to be tracked is automatically done by analyzing the GDOP each possible combination produces.

This receiver contains software for real time navigation. The navigator consists on an 8 state modified Kalman filter. It provides a solution in three spatial coordinates, three components of the velocity vector, as well as clock offset and drift (frequency offset).

The receiver clock is driven by a temperature compensated crystal oscillator (TCXO). This kind of oscillator is very inexpensive and low powered, compared to oven-enclosed crystal oscillators and more sophisticated clocks. This does not degrade the real time solution. The navigation filter is well designed, and clock offset and drift are accurately estimated, and position and velocity measurements corrected for them. But the clock behavior can be a major issue for high quality

measurements. In this situation, phase derived range, rather than pseudorange, is used to compute the solution in post-processing. This is precisely the area of the research that has been done, and reported here.

The receiver also can work in a differential mode. Corrections to measurements, rather than to solutions, can be input to the receiver, following the RTCM-104 standard format [Ref. 6].

This receiver was first conceived as a GPS upgrade to the Magnavox 4102 Transit Navigator, i.e., as a GPS sensor for an existing piece of hardware [Ref. 7:p. 1]. Neither control nor data logging can be achieved without an external device. But the receiver works on its own, automatically providing solution, as well as raw measurement output. The next section will be devoted to its interfaces.

The above mentioned characteristics, as well as a very high level of integrated circuitry, allowed the manufacturer to build the MX4200 at a very low cost (just over $3000), small sized (18x14x4.5 cm, 0.9 Kg) and with very low power requirements (10 to 32 Vdc, 5 watts max.) [Ref. 7,p. 1].

The antenna is a quadrafilar helix in an all weather case (19 cm high, 8.3 cm diameter) with no ground plate. For navigation applications, this is a desirable characteristic, to avoid loss of satellites when roll/pitch occurs. But it has its trade-off for ground applications, because it is more vulnerable to multipath effects.

B. INTERFACES

Four different interfaces have been established: Control port, Raw Data port, Equipment port and RTCM port. In addition, a timing pulse can be output once a second. It allows external devices to reference their measurements to GPS or UTC time.

1. Control port

This is an I/O interface to allow the control of the receiver functions, from an external device. The navigation solution is output through this port as well. A piece of software is provided by the manufacturer to perform this operation from an external IBM-PC computer, connected to the receiver through the control port. The external computer then becomes the Control and Display Unit (CDU). Under this configuration, several options in the receiver are accessible to the user:

- Initialization: input of approximate coordinates to facilitate the lock-on process.
- Rejecting undesired satellites.
- Time frame selection (GPS, UTC)
- Navigation mode: 2-D, 3-D, altitude aiding.
- Elevation mask for tracked satellites.
- Time recovery option.
- Requesting ephemeris and almanac data in the GPS message.
- Selection of desired records in the raw data stream, to be sent to the raw data port.

- Enabling/disabling differential corrections.
- Changing the dynamic response of the navigation filter.

Also, a continuous display of the status of the receiver, tracked satellites and navigation solution is available. Current navigation solution, differential corrections, almanac and ephemeris data, can be also recorded in the CDU.

2. Raw data port

This interface allows the user to access the raw data measurement, as well as navigation solution and time recovery data. It can be connected to an external IBM-PC computer to log those data. Almanac and Ephemeris, as well as several status and debugging messages, are output through this port, too. A description of their contents and meaning is given in the next chapter.

3. Equipment port

Allows the receiver to communicate with external navigation devices, following the NMEA-0813 Standard for interfacing marine electronics. Position, velocity and time can be sent to those devices through this port.

4. RTCM port

Inputs the corrections to the measured pseudoranges as received through a data link, following the standard RTCM format. Corrections, then, can be applied, real time, to the measured pseudorange, in a differential navigation mode.

C. NAVIGATION MODES

The navigation filter can compute the real time solution in different modes, as a function of the number of available SV's. The computation of the components of the state vector in the Kalman filter is prioritized as follows:

If 4 SV's are being tracked, measurements on their codes and carrier phase provide information to get a deterministic solution for the entire state vector. In fact, a deterministic solution is only obtained at initialization, if four SV's are available. The Kalman filter is a Least Squares Adjustment algorithm that uses the recent history of the solution as extra information to get the current solution. So, even if only four SV's are available, the solution is not truly deterministic. More than 4 SV's add redundant observations, so the reliability of the solution increases.

The user is allowed to fix the height of the antenna, which is fairly well known in a sea environment. Then, three SV's is enough to get a deterministic solution. Height and upwards velocity are not solved for, i.e., only a 2-D position and velocity solution is obtainable. Transition from 3-D to 2-D solutions is automatically done by default, if the receiver was set to 'auto' altitude aiding mode.

When the measurements are so few that the system is under determined, the Kalman filter keeps a 'dead reckoning' (DR) navigation mode.

The selection of the satellites to be used in the solution is based upon limiting values of elevation mask, VDOP and HDOP the user enters as a part in the initialization process. In addition, the user can modify the dynamic response of the navigator. The navigator then filters the measurements as a function of limiting values in horizontal and vertical accelerations.

D. TIME RECOVERY

This option directs the receiver to take the measurements at nearly even seconds of GPS time. This is done by adjusting the local physical time frame by the results of the Kalman solution. In addition, a timing pulse is output once a second.

Measurements are taken at certain epochs in the receiver time frame, i.e., in the time as kept by the receiver clock, instead of the GPS time frame. This is known as a 'user time receiver' [Ref. 7:p. 3]. When time recovery (TR) is disabled, measurements are taken at even seconds in the receiver time frame. When enabled, they are taken as close to an even GPS second, as the receiver is able to determine, based in the previous solution. This makes it possible, not only to have the timing pulse referenced to GPS time, but also to know the instantaneous clock offset and drift at that precise time. The navigation solution corresponds to the time when the pulse was output, so the receiver reports what was the status of its clock at the very instant of the pulse just sent. At the same

time, the last solution is used to compute when, in the receiver time frame, the next measurements must be taken.

E. THE MEASUREMENT PROCESS; TRACKING LOOPS

The receiver operation is based on two major components: tracking loops and the navigation filter. Each one runs on its own, with an interface in between which sends the measurements from the tracking loop to the navigator, whenever the latter requests them.

1. Tracking loops

Most of the information here contained should be credited to Keegan [Ref. 7] and has been experimentally verified, as shown in next chapter. A simplified discussion will be presented here.

The uppermost part of Figure 2 shows a schematic view of the tracking loops. At a first stage, carrier frequency is removed from the incoming signal. It is generated by the main oscillator, at the nominal L1 frequency. The frequency error in the receiver clock is then transferred to the Doppler frequency that is left.

A replica of the tracked code is generated. The code is then removed by multiplying that replica, properly delayed, by the signal. If that delay was well computed, the cross-correlation between both signals is one, so only a continuous wave of f_d frequency, modulated by the data, is left.

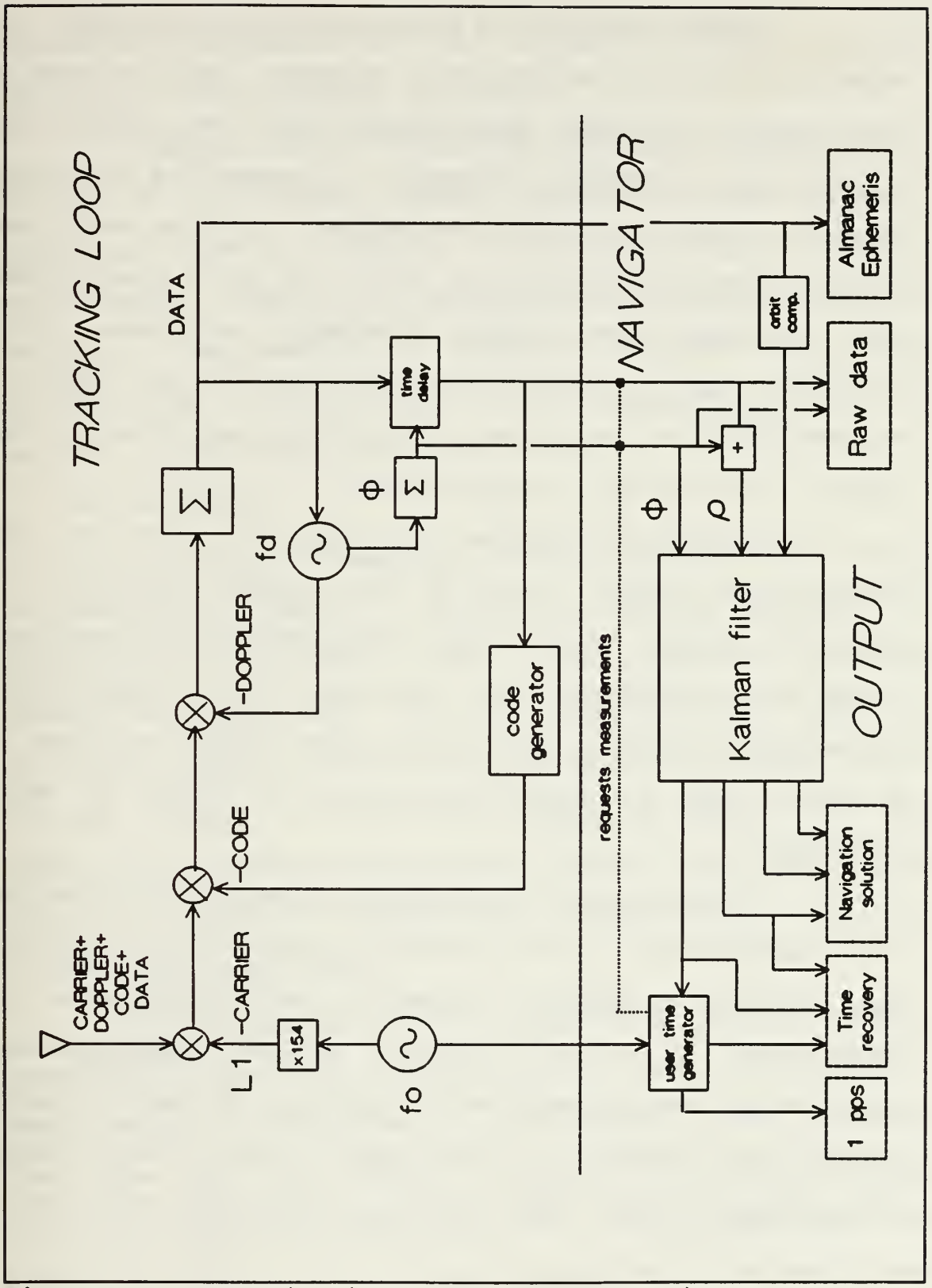

Figure 2. Schematic view of the MX4200 receiver.

Doppler frequency is then removed by multiplying the signal by a continuous wave of f_d frequency. Only the data is left, plus an additional error signal due to the mismodelling of time delay and Doppler frequency. By integrating this error signal in the correlator, corrections to time delay and Doppler frequency are computed. Then, they are fed back to the code generator and Doppler frequency oscillator. This oscillator also drives the code generator, so the signal is reconstructed at the proper chip rate, according to the Doppler shift in the incoming signal.

In addition, Doppler frequency is integrated once tracking was locked. Scaled by the carrier wavelength, it forms the current 'phase range' measurement. This integrated phase is then applied to the time delay. So, the code replica is generated with a $(t-\phi/f_{L1})-t_x$ time delay, relative to transmit time t_x, rather than $t-t_x$, as usual in other receivers.

In this way, all the relative dynamics SV-receiver has been removed from the code. Tracking, thus, can be done in a much narrower bandwidth, increasing the reliability of the measurement. It is the difference between pseudorange and phase range that the code loop is tracking. Its small dynamics allows for filtering the code signal (which is much noisier than Doppler) with a time constant quite large. This kind of

hardware architecture is well suited for code tracking, despite a relatively poor oscillator.

Another point of interest in the receiver architecture is that all the channels process precisely the same samples, which are taken in a common A/D circuitry. This makes the measurements virtually simultaneous for all the channels. In addition, measurements are taken at receiver clock time epochs; thus, the navigation filter can easily solve for receiver clock offset and drift.

2. Navigator

The navigator basically consists of the Kalman filter and associated logics to compute the desired epoch of the measurement. The inputs to the filter are time delay and Doppler frequency shift from the tracking loops, properly scaled to range and velocity. SV position and velocity, after the data message, are input in the navigation filter, too. The output is the position and velocity vectors, and clock offset and drift, relative to absolute GPS time and nominal frequency of the clock (10.23 Mhz).

The measurement epoch is computed in different ways, depending on the time recovery option. If it is disabled, measurements are requested at even seconds in the receiver time frame. When time recovery is enabled, the offset between the last measurement epoch and the corresponding even GPS second is computed. This offset is quantized to integer clock

cycles. The next measurement is then requested after a user time interval computed as follows: one whole second in the receiver clock minus the last computed offset. In other words, after 10,230,000 cycles minus the number of cycles corresponding to the computed offset at the previous epoch. The clock cycle is precisely the period of the local oscillator, or 1/10,230,000 = 97.7 ns.

In this way, the navigator is guaranteed to get the next set of measurements at the clock cycle transition that is expected (from the measurements at the previous epoch) to be the closest to the next even GPS second. When the solution corresponding to the next epoch is computed, the receiver will report, in addition to the solution itself, how many clock cycles the measurement epoch was shifted, relative to the receiver clock cycles counter.

F. SOFTWARE AND FIRMWARE

As a brand new piece of hardware, the receiver, as well as its supporting software, is subject to some upgrading. Most of the research was done on data from receivers with a D020 firmware version. Some of them were taken with an older version, D011. The major difference between them is the time recovery option, not available in the D011 version. Data formats are slightly different, too.

Two different CDU software versions were used, too: version 1.01 and version 1.06. The main difference is the

ability of version 1.06 to control the data flow in the raw data port. Unless specifically stated, all the information here contained, refers to firmware version D020 and software version 1.06.

IV. THE RAW DATA MESSAGE AND THE COMPUTATION OF THE MEASURABLES

This chapter is devoted to the contents of the raw measurement records, and how all the numbers should be combined to build the actual measurements. The goal of the research is to characterize the physical clock of the receiver. Because of the high rates of drift in the clock, the receiver has been provided with the Time Recovery option. It means that the receiver can slew the time of the measurement to keep the offset, relative to the GPS time, at the 30 meters (100 ns) level. That makes it possible to take simultaneous measurements with different receivers. But if time tags are being adjusted, all the measurements taken at a given epoch will contain the jump corresponding to that adjustment. Let us see first how the variables are reported, to see then how the measurements should be computed. Finally, the effect of the time tag adjustment on the reported measurements will be discussed.

A. THE MX4200 RAW DATA MESSAGE

All the quantities involved in measurements, solution and time recovery are output by the receiver through its raw measurement port. They are reported in record types 1 or 2, 8 and 969 respectively. [Ref. 8] gives a description of them.

1. Raw measurement data record, types 1 and 2

The raw measurements come out in one of two operator's selected format. Block 1's have the data for one satellite at a time. Block 2's are compressed version of block 1's and contain the information for all the channels at a time. Block 2's take about one sixth the space as the equivalent data in block 1's. Although block 2's contain only printable characters, the data is not meaningful till it has gone through an expansion algorithm.

Listed in Table 1 is a sample of a raw data set, in a block 1 format, with all its variables named.

TABLE 1 RAW DATA RECORD AND ITS CONTENT

ID	CH	PRN	USR_MS	CHL_MS	PHI	CODE	PHFR	CR	SNR	H
1	1	17	353520000	353519920	16478859	128	-44	124	43	+
1	2	20	353520000	353519919	8595657	114	-12	123	42	-
1	3	23	353520000	353519919	3547947	25	72	125	43	-
1	4	16	353520000	353519919	9408528	96	-115	125	43	+
1	5	3	353520000	353519918	20774479	138	-119	125	42	-

Name	Description
ID	Record type, 1
CH	Channel number
PRN	PRN or satellite identifier
USR_MS	User time of measurement, milliseconds
CHL_MS	Channel or transmit time, integer milliseconds
PHI	Integer number of L1 cycles, integrated carrier phase
CODE	Raw code offset, in integer number of L1 cycles
PHFR	Fractional part of integrated carrier phase in units of 1/256 L1 cycles
CR	Costas ratio: estimate of maximum error in phase measurement
H	Half-cycle ambiguity resolution indicator

Several issues should be pointed out here:

- Reported receiving and transmit time are in different time frames: 'User time' and 'GPS time' respectively.
- The +/- sign at the end of each record is described in [Ref 7:p. 4] as a half-cycle phase indicator. This resolves the half a cycle ambiguity in the phase measurement. When a - sign is reported, half a cycle should be added to the resulting phase measurement
- For a record type 2, USR_MS and PHI are reported in a slightly different way that in block 1's.

2. Solution record, type 8

Table 2 shows a solution record with all its fields named as the variables they represent.

TABLE 2. SOLUTION RECORD AND ITS CONTENT

ID	TREC	LAT	LON	HT	VN	VE	VU	VCK	M	N	DP
8	353513.00	36 35.9357	-121 52.5952	-49.3	0.0	0.0	-0.0	86.6	3	5	6

name	Description
ID	Record id., type 8
TREC	Receiving time in seconds within the week
LAT	Latitude, degrees and minutes, WGS 84 Reference System
LON	Longitude, same as before
HT	Height above the ellipsoid, meters
VN	North velocity component, meters per second
VE	East velocity component
VU	Upwards velocity component
VCK	Clock drift, meters per second
M	Navigation solution mode (DR, 2-D, 3-D)
N	Number of satellites concurrent in the navigation solution
DP	Geometrical Dilution of Precision

Several items to note are:

- Receiving time, TREC, can be optionally reported in UTC or GPS time. The solution block following the data that generated it, will have a time tag several seconds smaller than the data if UTC is selected (the default).

- Solutions will be at even seconds when time recovery (TR) is on. TREC will show the clock offset if TR is disabled. When a navigation solution cannot be computed, the TR offset is held fixed.

- The number of digits in each field limits the resolution of the navigation solution: 1/10000 minutes in latitude and longitude, a decimeter in height and one tenth of a meter per second in velocity.

- CKV is the clock frequency drift, as computed by the Kalman filter, scaled to m/s.

3. Time recovery record, type 969

The receiver can output a timing pulse every second, when is set to 'time recovery'. Under these circumstances, record 969 provides useful information about the estimated accuracy of that pulse and status of the receiver clock. Table 3 shows its contents. Most important for post processing, this record contains the information about the adjustment the receiver has made to its internal clock.

TABLE 3. TIME RECOVERY RECORD AND ITS CONTENT

ID	CLKMV	FOFF	CLKOFF	ERR
969	-87.916	-455	-0.000000615	41

Name	Description
ID	Record id., type 969
CLKMV	'Clock moved' last time of measurement, in meters
FOFF	Frequency offset of receiver clock, relative to L1 carrier frequency, cycles
CLKOFF	Receiver clock offset from GPS time
ERR	Error in the last time pulse, in units of the local oscillator period (10.23 Mhz)

FOFF (frequency offset) corresponds to VCK in a position record, expressed in cycles of the L1 frequency. ERR (error in the last time pulse) has to do with hardware delays

in generating the timing pulse and is not pertinent to this analysis.

CLKOFF (clock offset) is the last estimated error in the 'corrected' internal clock at the last measurement epoch. When solutions are not computed, CLKOFF stays at the last computed value. Finally, CLKMV ('clock moves') is the amount of time the clock was adjusted prior to the last measurement. It is given in units of length.

B. COMPUTATION OF THE MEASURABLES

Let us examine how to compute the raw measurements (pseudorange and phase-derived range) from the quantities reported in the raw data message. Time recovery will be assumed off. How enabling TR affects the measurement computation will be discussed later.

The MX4200 Technical Manual provides an algorithm to compute pseudorange and phase range from the reported quantities in records type 1 [Ref. 8:p. C-4]. It refers to B003 and D003 firmware versions:

$$\rho_{\phi} = -(PHI + \frac{PHFR}{256})\ \lambda \qquad (16)$$

$$T_r = \frac{USR\_MS}{1000} \qquad (17)$$

$$T_x = \frac{CHL\_MS}{1000} - \frac{\rho_\phi}{c} + \frac{CODE}{f} \quad (18)$$

$$\rho = (T_r - T_x)\ c \quad (19)$$

where

- $\lambda = c/f$ = L1 carrier wavelength
- c = speed of light, 299,792,458 m/s
- f = L1 carrier frequency, 1575.42 MHz
- T_r = receiving user time
- T_x = transmit GPS time
- ρ = pseudorange
- ρ_ϕ = phase-derived range, or biased phase range.

The April 1991 Firmware Release Announcement [Ref. 9:p. 4] adds a new issue to the measurements computation for the upgraded B020, D020 and N020 firmware versions: half a cycle should be added to the reported phase, when the half cycle indicator, H, is '-'. Then, reported phase measurement will be:

$$\phi=(PHI+\frac{PHFR}{256}+a\frac{1}{2})\quad cycles,L1\ frequency \quad (20)$$

where a is one when H is '-', 0 otherwise.

Let t_u, t_x be the reported USR_MS and CHL_MS, as expressed in seconds:

$$t_u = \frac{USR\_MS}{1000} \tag{21}$$

$$t_x = \frac{CHL\_MS}{1000} \tag{22}$$

and, finally, let Γ be the reported CODE, in L1 cycles. Then, expressions (16) to (19) become:

$$\rho_\phi = -\phi\lambda \tag{23}$$

$$T_u = t_u \tag{24}$$

$$T_x = t_x + \frac{\phi + \Gamma}{f} \tag{25}$$

$$\rho = (T_u - T_x)c \tag{26}$$

Let us see now that the reported ρ_ϕ is in fact the phase range, biased by the integer milliseconds t_u-t_x. As will be seen, the pseudorange is computed as the sum of the phase range and the small value CODE. This is a consequence of the phase aided code tracking loop, described in Chapter III.

The measured range is in fact

$$\rho = \Delta t \; c \tag{27}$$

where Δt expresses the time delay between transmit and receiving time of a given edge of the code that modulates the signal. It is measured in seconds of physical time. This kind of seconds cannot be realized other than by means of a count of clock cycles.

When the tracking is first locked, the number of cycles the replica was delayed can be scaled by 154 (which is the number of L1 cycles in a clock cycle). So, the measured range can be expressed in terms of an integrated Doppler phase, i.e., carrier cycles:

$$\rho_0 = \phi_0 \, \lambda \tag{28}$$

where ϕ_0 is 154 times the number of clock cycles, and λ is the carrier wavelength. The error in the first measurement will be propagated to all the measurements thereafter. It is the bias in the phase derived range. The initial phase count can be split into two parts: an integer number of milliseconds, by excess, minus a submillisecond phase count:

$$\rho_0 = \frac{M_0}{1000} c - \phi_{ms,0} \lambda = m_0 c - \phi_{ms,0} \lambda \tag{29}$$

Here M_0 is the initial integer number of milliseconds, and m_0 is the same quantity, expressed in seconds.

The output from the correlator is used to correct the Doppler frequency and time delay models, so the process is self sustained. The change in range to the satellite is measured by integrating the Doppler frequency. It is added to the previous ϕ_0. Because the propagation medium is dispersive, phase velocity is larger than group velocity. Therefore a time delay equivalent to that Doppler count will not be enough to get maximum output in the correlator. An extra time delay is introduced, and this is known, in the Magnavox notation, as CODE (Γ), reported in carrier cycles. Then, after a certain interval, the range can be represented by

$$\rho_i = m_0 c - (\phi_{ms,0} + \Delta\phi_i + \Gamma_i)\lambda = m_i c - (\phi_{ms,i} + \Gamma_i)\lambda \qquad (30)$$

Here m_i is an integer number of milliseconds. The range measurement is thus divided into a whole number of milliseconds and a count of extra cycles. Whenever $\phi_{ms,i}$ gets to zero cycles (or to 1,575,420 if the range is increasing), it is reset to 1,575,420 (or to 0). At the same time, a new millisecond is added (or subtracted) to m_i. Figure 3 shows how those milliseconds adjustments in phase are done. The jagged curve at the bottom is what the receiver reports as phase, scaled to range. If that reported phase range is subtracted

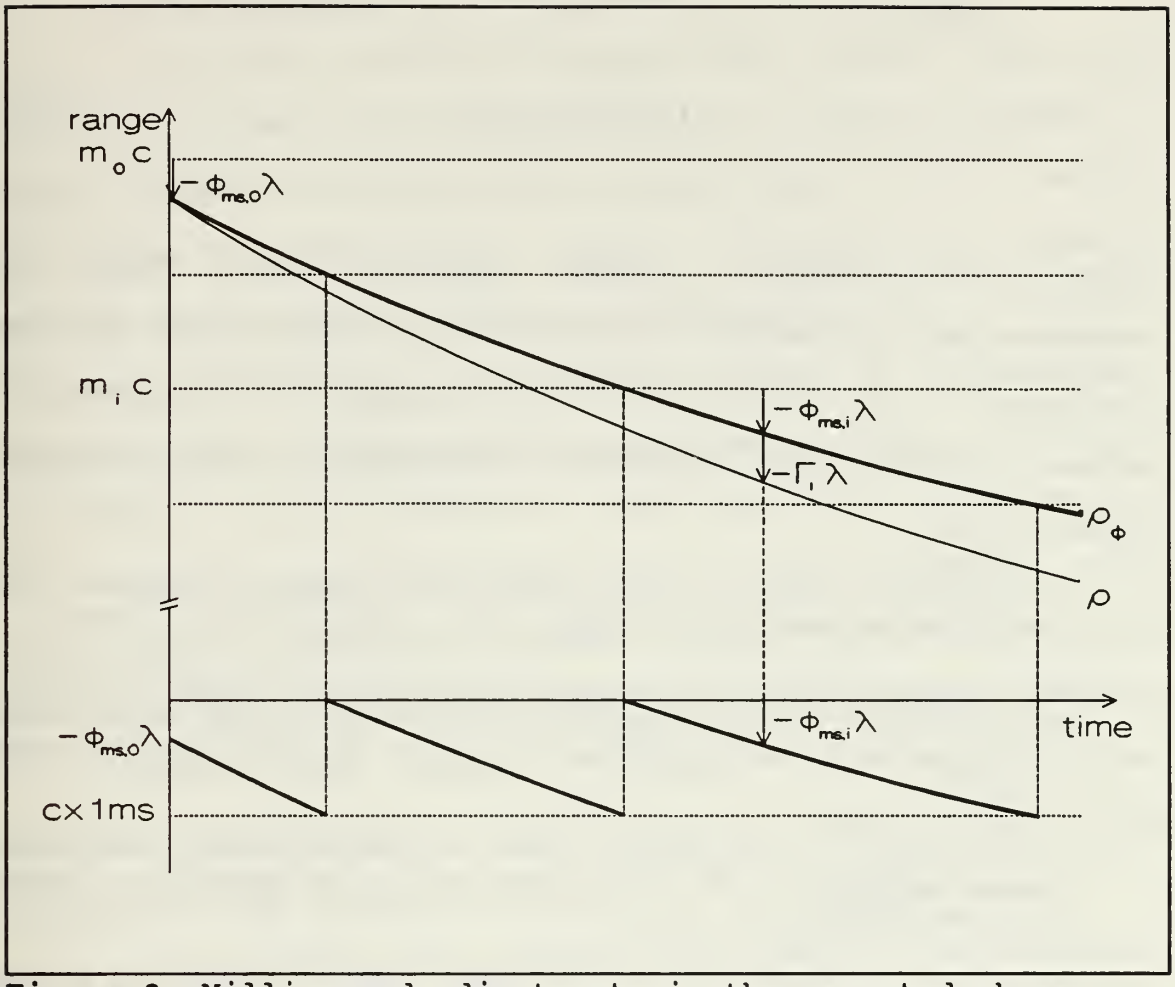

Figure 3. Millisecond adjustments in the reported phase

from the range corresponding to the integer number of milliseconds, the uppermost curve, phase-derived range, is obtained. Thus, eq. (16) and (23) should be properly adjusted to have the actual phase derived range:

$$\rho_\phi = (t_u - t_x)c - \phi\lambda \qquad (31)$$

If in addition, the CODE range equivalent is subtracted from the phase derived range, the pseudorange is obtained, i.e., the ρ curve in Figure 3.

Code

$$\Gamma = \frac{1}{\lambda}(\rho_{\phi} - \rho) \qquad (32)$$

gives the difference between measured phase range and pseudorange. The hardware architecture, thus, allows the code component of the loop to track only changes in the difference between biased phase range and pseudorange. This difference consists of:

- Ionospheric delay, that enters with opposite sign in the phase measurement and range (time delay) measurement.
- Multipath effects, that are different for phase and code, too. Their interference patterns are not alike because the difference in wavelengths of carrier (0.19 m) and C/A code (300 m).
- Difference in the noise level of pseudorange and phase measurements. It is about two orders of magnitude larger for pseudorange.
- Finally, it contains the original bias in the phase range.

These effects, combined all together, have a much smaller dynamics than the actual range to the SV. Thus, it is possible to keep it tracked in a much narrower bandwidth.

C. RAW VERSUS REPORTED MEASUREMENTS

Let us see now how to set the receiver to time recovery option affects the reported measurements, so we can adjust them.

1. Three different time frames

In the literature dealing with precise time, two different concepts are common: 'physical' clocks as opposed to 'paper' clocks. Let as assume we have a wall clock to watch, that lags an indeterminate number of seconds in a certain period. Current time is going to be requested once in a while. To deal with that lag, we carefully listen to the broadcast timing signals in WWV. At the same time, we keep a record of the number of even seconds our wall clock lags. Whenever time is requested, we will report what our wall, physical clock says, plus the number of seconds we know for sure it lagged last time the record was updated. This whole process is known as a 'paper clock'. Neither of those two times is true time, which is only known at timing signal epochs. Then, three different time frames are present in the example above.

There are three different time frames in the receiver, too:

- Absolute time, corresponding to GPS time in this case. It is only estimated whenever the receiver gets a navigation solution. The estimate has enough accuracy to decide how many cycles the measurement epoch lags the GPS time. This corresponds to the absolute time in the example above. Absolute time will be represented by T_s.
- Physical time, that is kept by the receiver physical clock; it is driven by a freewheeling oscillator, at a nominal frequency 10.23 Mhz. It is represented by T_p.
- Paper time: this is the time the receiver reports in the data stream, as the time of the measurement. This is known as user time and will be expressed as T_u.

Measurement epochs are at even seconds in user time. But user time is an artifact. The receiver needs to compute when, in its physical clock time, the measurements are to be taken. That is, precisely at which transition of the physical clock counter.

The cycle of measurement and time adjustment begins with a navigation solution. The estimate of the clock offset and drift (from navigation solution) are used to predict the number of physical clock counts between the last measurement and the next true GPS second mark. The difference between this value and the nominal count of N_0 = 10,230,000 (one second at 10.23 MHz), is the value δ reported in the 969 record, i.e., CLKMV (δ in fact has been scaled to range, to be reported as CLKMV). When the last measurement was taken, the cycles count was reset to zero. The next measurement will be taken when the cycle counter of its physical clock gets to $N_0 + \delta$, i.e., at a physical time

$$T_{u,i+1} = T_{u,i} + \frac{N_0 + \delta_i}{f_0} \qquad (33)$$

The same process occurred in the previous measurement epoch, so this number of cycles has been added to the previous clock shift. This is

$$\Delta_i = \sum_{j=1}^{i} \delta_j \tag{34}$$

and

$$T_{u,i+1} = T_0 + (i + 1) + \frac{\Delta_i}{f_0} \tag{35}$$

Because no offset existed at initial time

$$T_{p,i+1} = T_0 + i + 1 \tag{36}$$

so

$$T_{u,i+1} = T_{p,i+1} + \frac{\Delta_i}{f_0} \tag{37}$$

Figure 4 shows the relationship between these three time frames. T_g is the true GPS time; the interval between $T_{g,i}$ and $T_{g,i+1}$ is precisely 10,230,000 times the nominal period of the oscillator. Once the receiver has a measurement, at $T_{u,i}$ (which is an even second in user time), the time and frequency offset in the navigation solution are used to compute δ_i, i.e., the number of cycles for the next measurement epoch to be shifted.

A new cycles count starts then and the next measurement will be taken after $N_0 + \delta_i$ cycles. Cycles in the

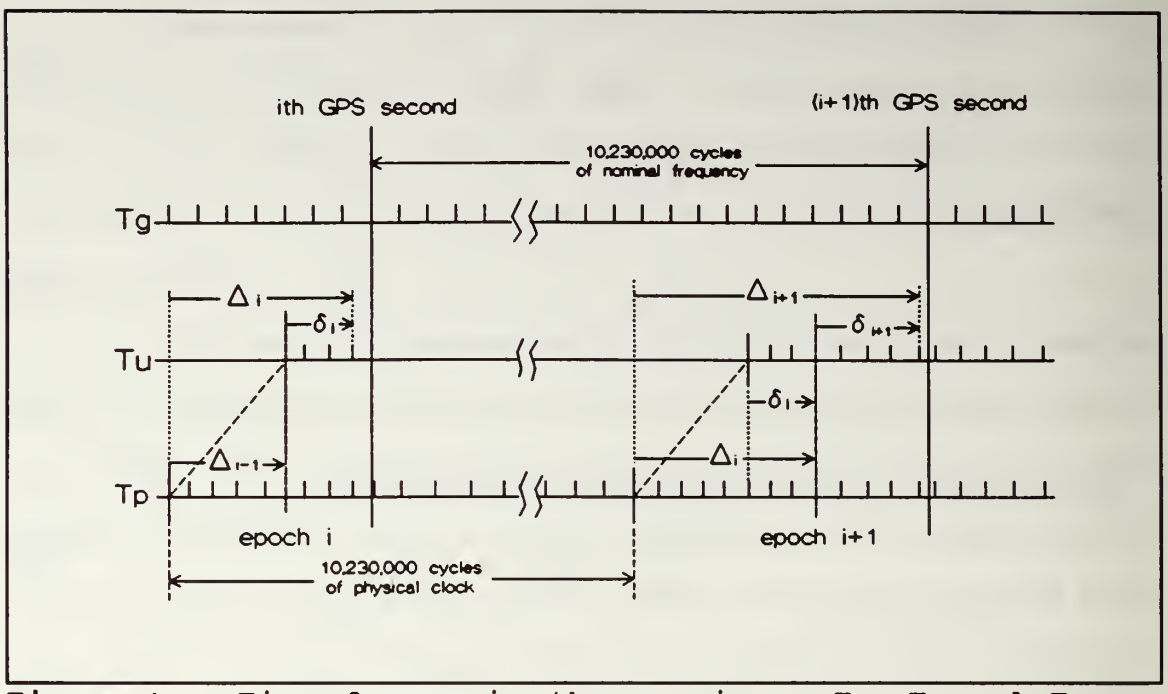

Figure 4. Time frames in the receiver. T_g, T_u and T_p are 'GPS', 'user', and 'physical' time respectively. δ_i is the clock shift at epoch i+1. Δ_i is the integrated clock shift.

physical clock do not have precisely the same period, though. When that count gets to the end, and a new measurement is taken, a different δ_{i+1} estimate is found. The next measurement will be taken after $N_0 + \delta_{i+1}$ cycles of the physical clock.

2. Raw measurements computation

The noise in the physical clock of the receiver is the subject of the research. In a Time Recovery off situation no clock shifting is done. Thus, both measurements and time tagging are expressed in terms of the physical clock readings. User and physical times are synonymous.

Contrarily, if Time Recovery is on, the time of the measurement i has been shifted by Δ_{i-1} cycles, with respect to

the physical time. The time tagging process is driven by the physical clock. The timing error is the error in the physical clock. Thus, to compute it, we need the reading of the physical clock to which Δ_{i-1} has been added to get the measurement epoch, i.e.

$$T_{p,i} = T_{u,i} - \frac{\Delta_{i-1}}{f_0} \tag{38}$$

Now, if the measurement epoch has been delayed until $T_{u,i}$, the measurements at that epoch, as expressed in terms of user time, have been biased by the range corresponding to Δ_{i-1} cycles:

$$\begin{aligned} \rho_{\phi,b} &= (T_u - T_x)c - \phi\lambda \\ &= (T_p + \frac{\Delta_{i-1}}{f_0} - T_x)c - \phi\lambda \end{aligned} \tag{39}$$

Thus, to retrieve the raw measurements, the same adjustment should be done:

$$\rho_\phi = (T_u - T_x)c - \phi\lambda - \frac{\Delta_{i-1}}{f_0}c \tag{40}$$

and the same applies to the pseudorange. By comparing these ranges with the true ranges it is possible to see the error in the physical clock.

Now, raw measurements can be obtained in terms of the reported quantities as follows:

$$\rho_{\phi} = \left(\frac{USR\_MS - CHL\_MS}{1000}\right) c - \left(PHI + \frac{PHFR}{256} + a\frac{1}{2}\right)\lambda - \sum_{j=1}^{i-1} CLKMV_j \qquad (41)$$

$$\rho = \rho_{\phi} - CODE\ \lambda \qquad (42)$$

regardless the Time Recovery option that was selected. The physical time corresponding to that epoch will be:

$$T_{p,i} = \frac{USR\_MS}{1000} - \sum_{j=1}^{i-1} CLKMV_j \qquad (43)$$

V. CHARACTERISTICS OF THE RECEIVER CLOCK

From the information contained in Chapter IV, it is possible to retrieve the raw measurements the receiver performs. They are contaminated by many different biases and errors. Those external to the receiver are not the main issue here. They should be removed from the measurements, prior to the analysis, though. It is mainly the clock characteristics which determines the accuracy in the measurement. This will be the subject of the present and next chapters.

A. DETERMINISTIC EFFECTS PRESENT IN THE MEASUREMENT.

All those effects present in the measurement that can be somehow modeled, will be considered as deterministic. Stochastic noise, on the other hand, cannot be modeled. Their sources may be identifiable as either noise or unremoved biases. They can only be quantified as a bulk.

1. External to the clock

All those biases, mentioned in Chapter II, as due to the satellite (clock bias, position and velocity) and the propagation medium (ionospheric and tropospheric delays), are considered here as deterministic effects external to the receiver clock.

2. Internal to the clock

The accuracy of a clock is the deviation of its reading from an absolute time. In a general sense, this accuracy can be expressed as a polynomial of a certain degree in Δt, plus a stochastic noise component.

That polynomial, that models the bulk of the clock accuracy, is considered as the deterministic part of the clock error. The order of the polynomial needed is highly dependent on the stability of the clock and the elapsed time since synchronization. As a matter of experience, up to a third degree polynomial model should be attempted for this particular clock, and half a day span of time. A quadratic model would be enough for periods shorter than one hour. Later on it will be seen that some effects of temperature change can be present. Its effect is very hard to separate from those due to the physical characteristics of the particular crystal in question.

In addition to that, Hellwig [Ref. 10:p. 27-30] gives four main deterministic effects in crystal oscillators. Only the two first were studied here:

- Temperature.
- Transient regimes.
- Gravitational forces and accelerations.
- Line voltage variations.

B. THE CLOCK MODEL

As a fundamental analysis tool, a FORTRAN program was written to calculate a model of the receiver clock offset, relative to GPS time. It is based on the recorded raw measurements, in a given observation session. Appendix A, contains a description of it.

This program calculates a model of the deterministic part of the clock behavior. In addition, a further characterization of the stochastic noise is possible. It is done by analyzing the residuals of the raw measurements, from that model. This will be the subject of Chapter VI. Underlying this procedural scheme there is an assumption: all the deterministic effects, other than the clock stability, are not present in the measurements. To achieve this, three different approaches can be taken, according to each particular effect:

- To fix the conditions under which the measurements were taken, so some of the effects could be considered as negligible. In particular: receivers at rest, fed by a well stabilized power supply, well off transient regimes, and carefully watched temperature variations.
- To subtract from the measurements a model of every identifiable (and modellable) effect: true range to the corresponding SV and a Hopfield tropospheric delay model.
- For ionospheric delay, whose models are not very reliable, just assume its effect as negligible. Spread over the entire visible constellation of SV's, it introduces a small, unknown bias into the clock offset. No significant effect is introduced in the frequency offset; it can be considered as a secular variation over a SV pass.

Not meeting any of these conditions may lead to a model or noise characteristics dominated by the particular condition

lacking. On the other hand, modifying only one of these conditions allows its effect on the clock to be estimated. Experiments on temperature variations, the effect of ephemeris changes and SA activation on the noise, and duration of the transient regime were done. They will be discussed later.

A description of the program MXCKMO is given here to show how all the issues above were taken into account. It is linked to several routines in the GPS packages FIC5, GAPP5 and GEN5 by the Applied Research Laboratory, University of Texas at Austin. They are listed in Appendix B, and a brief description of them will be given. Several other low level routines, such as data decompression, extraction of ephemeris and data logging, were written by Dr. James R. Clynch. They are used here as interfaces between the receiver output and the main analysis program. They are listed in Appendix C.

1. Data logging

An initial problem was found in the raw data stream. Clock shifts are given in instantaneous values, at measurements epochs. As shown in eq. (41), integrated values are required to retrieve the raw measurements.

To avoid logging all data, for sessions lasting a few hours, a new routine was needed. MXR adds all the reported clock shifts, up to the current epoch. The result is saved, as integrated clock shift, in a new field added to the 969 record. In addition, MXR selects entire blocks of 1/2, 8 and

969 records to be logged, at a user's choice epoch interval. Other useful records, such as ephemeris and almanac, can be recorded, too, taking advantage of the user's ability to request their output from the CDU.

2. Data interface

Once the raw data are recorded, the MX42RTN package performs several operations on them. One routine allows a sequential extraction in entire blocks of raw data, navigation solution and time recovery, corresponding to the same epoch. Among those operations, decompression of records type 2 and ephemeris and almanac records are key items. Ephemeris data can be converted to FIC binary format, and saved in a file by means of the program MX2EPH. Several routines in the FIC5 and GAPP5 packages (LOADTAB, GETEPH, FINDEPH), handle them in an efficient way. The whole ephemeris set is loaded in a 20x3x130 array. The desired items are fetched in RAM, rather than in files.

3. Input interface

This allows the user to enter all the parameters for the computation. In particular, the following are prompted:

- Names of data, ephemeris and output files.
- Initial and final epochs for the computation to be completed.
- Reference time of epoch and degree of the polynomial model.

- Specification of PRN's to be removed from the model computation. It can be useful whenever a given SV inputs undesired effects in the computation.

- Specification of PRN's for which output files are not desired. MS FORTRAN 5 imposes a limitation in the number of files can held simultaneously open.

- Selection of the ground position from those stored in the STATIONS.FIL file. LOADSTA routine, in GAPP5 package, allows the retrieval, coordinates transformation and storage in memory, of the antenna position.

- Surface meteorological data, to be used in the ANLTROP function (GAPP5). This is a Hopfield tropospheric model.

4. Main algorithm

The algorithm is based on the computation of the coefficients of a polynomial. It models the physical clock offset, relative to GPS time. At a given epoch *i*, that offset is first estimated by comparing measured pseudorange to the satellite, with the true range. The same process is done for all the available satellites at that epoch (except those specifically excluded from the model computation). Between initial and final epochs, all the range residuals are computed. These observed-minus-computed ranges (OMC's), scaled to time, enter in a batch Ordinary Mean Least Squares Adjustment (OMLS) to find the coefficients of the polynomial that better fits them. The adjustement process is described in Appendix D.

Five main components can be identified within the main algorithm: Raw data input, receiver clock correction, OMC computation, computation of the deterministic model and statistics.

a. Raw data input

These data are read by calling MXRDRW routine. In turn, it loads an entire block of data by means of NXMX42 and M42SET (MX42RTN package). Raw measurements, uncorrected by clock shift, and the clock shift itself, are returned.

For data logged in TR option, the integrated clock shift at the previous epoch is needed. The routine selects integrated clock shift from either the previous or the current block, depending on the format of the measurements record. If raw measurements are in compressed format, the integrated clock shift in the previous block is needed. It is computed by subtracting the instantaneous clock shift from the integrated clock shift in the current block. If raw measurements are in ASCII format, the integrated clock shift at the previous epoch is in the current block.

Once the main program has the unadjusted (by clock shift) ranges and the clock shift, the raw ranges are computed following eq. (41) and (42). The reading of its physical clock, at that epoch, is also computed:

$$t_{p,i}=t_{u,i}-\frac{\Delta_{i-1}}{f_0} \qquad (44)$$

If TR was off, or navigation solution failed, Δ_{i-1} is 0. The measurements are taken at an even second of the physical clock for that case.

b. Receiver clock correction

The physical time of the receiver clock should be now corrected by its offset, relative to GPS time. This is done by means of the clock offset model computed in the previous iteration. The model

$$\tau(t)=a+b(t-t_0)+\frac{c}{2}(t-t_0)^2+\frac{d}{6}(t-t_0)^3 \qquad (45)$$

is expressed in terms of a GPS time interval. It might be known only to within a few tenths of a second. But t (GPS time) is

$$t=t_p-\tau(t) \qquad (46)$$

Then, τ is first computed as

$$\tau^1=a+b(t_p-t_0)+\frac{c}{2}(t_p-t_0)^2+\frac{d}{6}(t_p-t_0)^3 \qquad (47)$$

and then iterated as

$$\tau^i=a+b(t_p-\tau^{i-1}-t_0)+\frac{c}{2}(t_p-\tau^{i-1}-t_0)^2+\frac{d}{6}(t_p-\tau^{i-1}-t_0)^3 \qquad (48)$$

until

$$|\tau^i-\tau^{i-1}|\leq 10^{-12} \qquad (49)$$

Then pseudorange and phase range, as well as physical time, are corrected by this clock offset:

$$\rho_c = \rho_m - \tau c \tag{50}$$

$$\rho_{\phi c} = \rho_{\phi m} - \tau c \tag{51}$$

$$t_{pc} = t_p - \tau \tag{52}$$

c. OMC computation

To perform the computation of the true range, the closest ephemeris set to the current epoch is chosen. This is not a requirement for data sets spanning less than three hours. The elements of the broadcast orbit are claimed to be good within six meters and valid for four hours. They are updated every two hours.

For periods longer than three hours, the SV position must be computed with different sets of ephemeris. It has the effect of introducing spurious noise when switching from one to another. The difference between ranges, as computed with two consecutive ephemeris sets, is taken. This difference is then added to the new range, so the discontinuity is saved.

To compute the true range to the SV, the GPS time of the measurement is needed. Again, this is only known

approximately. Residuals off the clock model have been observed to be as much as 100 Km , i.e., 0.3 ms. The SV moves about 4 Km/s. At that velocity, a 0.3 ms error in time makes an error in the computed position of about one meter.

Actual GPS receiving time is:

$$t=t_p-(\tau+\epsilon)=t_{pc}-\epsilon \tag{53}$$

where ϵ is the residual from the clock offset model τ. The range to the SV is first computed at

$$t^1=t_{pc} \tag{54}$$

Tropospheric model correction is then applied to this computed range, so

$$r_c^1=r^1+d_{trop} \tag{55}$$

Then, a first estimate of the OMC and the time residual is computed:

$$\epsilon^1=\frac{\rho_c-r_c^1}{c} \tag{56}$$

This first residual is then added to the clock offset model. A better estimate of the true GPS time is then obtained,

$$t^2=t^1-\epsilon^1=t_p-(\tau+\epsilon^1) \quad (57)$$

and new true range and residual are computed. The process is iterated until the change in the residual is less than 10^{-12} seconds. The OMC so computed

$$\epsilon=\frac{\rho_c-r_c}{c} \quad (58)$$

is in fact the time residual corresponding to the given SV, at current epoch i, for the present iteration of the adjustment process.

The routine to compute the theoretical range follows an iteration scheme, too. It first computes the SV position and range for the input time, i.e., receiving time. Then, it computes transmit time by subtracting the time of flight, and corrects the ground position by Earth rotation. The process is iterated until convergence. Relativistic effects are corrected for, too.

d. Computation of the deterministic model

As residuals for each SV and epoch are being computed, a new observation equation is added to the system. The H^tH and $H^t\epsilon$ are being updated with new entries every time a new measurement is processed. For N observation equations, the size of the elements in H^tH ranges from N to $Nx\Delta t^3$. For three hours worth of data, at one second logging rate, those

numbers are in the order of 10^4 and 10^{18}. H^tH is ill conditioned for inversion purposes.

The normal equations system

$$(H^tH)\vec{x}=H^t\ \vec{\epsilon} \tag{59}$$

is solved by LU decomposition [Ref. 11:p. 31-43]. Routines LUDCMD and LUBKSD, modified to double precision, were used.

The first solution to the system, $\vec{x}_0$ is iterated as

$$H^tH\ \vec{x}-H^tH\ \vec{x}_0=H^tH\ \Delta\vec{x}= \\ H^t\ \epsilon-H^tH\ \vec{x}_0 \tag{60}$$

so the system can be solved for $\Delta\vec{x}$ now, and

$$\vec{x}=\vec{x}_0+\Delta\vec{x} \tag{61}$$

Iterations are done until the change in the parameters is less than $10^{-(19+2j)}$, where j is the current iteration of the adjustment process. This guarantees a change less than 10^{-27} in the fourth iteration of the main process. For three hours worth of data, at 1 second rate, the change in the cubic term, worst case, would be less than $(5 \times 10^4)^3 \times 10^{-27}$, in the order of 10^{-13} seconds.

The convergence criteria for the adjustment process was set to halt the process when the variation in any

parameter would produce a clock offset increment lesser than 1 ns, worst case.

e. Statistics and edition of data

The raw data file might contain several anomalous records. They degrade the model computation. The main routine implements different algorithms to edit them out of the computation. Each computed OMC is tested against a window. The size of that window is reset to five times the a-posteriori variance of the residuals in the previous iteration. Pseudoranges failing this test are excluded from the model computation.

Statistics on the residuals after adjustment are given on a SV basis. It allows the user to exclude those SV's that show anomalous behavior, from a later model computation. Statistics on Doppler measurements also are done on a SV basis. Doppler measurements do not enter the model computation. Increment in phase range, between previous and current epoch, is computed every epoch. This difference, divided by the computed interval, gives the measured Doppler. The increment in true range, divided by the same interval, gives the true Doppler shift, corresponding to the true change of the SV position. The difference between them is called Doppler residual. It is, in fact, the frequency offset in the receiver clock, at the measurement epoch.

Some of the phase range measurements can be wrong. Then, both the current and next Doppler residuals will be in error. To avoid that problem, a dynamic window edits those anomalous measurements out of the statistics computation. The size of the window is reset once a new Doppler residual is computed. It is designed as a recursive filter of equation:

$$y_i = 0.1\ x_i + 0.9\ y_{i-1} \qquad (62)$$

where y_i, x_i are the smoothed and actual residuals. A rejected Doppler residual is flagged in the output file.

The way that record is flagged depends on the kind of anomaly found: acquisition, reacquisition, gap in the data or anomalous phase range. At a later stage in the analysis, that flag gives an indication on the confidence that should be credited to that measurement. This is helpful to decide whether or not to use that particular record for noise analysis purposes.

5. Outputs

One residuals file per selected SV is output. It contains the following items:

- Modeled GPS time of the measurement epoch.
- Phase-derived range residuals.
- Doppler residuals.
- Doppler residuals flag.

```
READ 10276 DATA RECORDS IN  1 TH LOOP

READ 10276 DATA RECORDS IN  2 TH LOOP

READ 10276 DATA RECORDS IN  3 TH LOOP
prn 12 switched to TOE  345600. eph. itm. at  336900.
prn 13 switched to TOE  345600. eph. itm. at  336900.
prn 15 switched to TOE  345600. eph. itm. at  336900.
prn  2 switched to TOE  345600. eph. itm. at  336900.
prn  6 switched to TOE  345600. eph. itm. at  336900.

READ 10276 DATA RECORDS IN  4 TH LOOP

PSEUDORANGE RESIDUAL STATISTICS PER SATELLITE :
     PRN          N. POINTS          AVG.          STD DEV  ( METERS )
     12              2042            5.81           16.672
     13              2096           -5.79           15.611
     15              1946            -.09           15.974
      2              2096           -3.73           15.047
      6              2096            3.96           15.849

COMPUTATION COMPLETED BETWEEN 336900 AND 339000 USING  5 SATELLITES:
               12, 13, 15,  2,  6,

4 ITERATIONS WERE DONE ON DATA FILE m22115.149

3 PARAMETERS CLOCK MODEL AT TIME OF EPOCH WN 594.  SOW  337950.:
-.144134995E-02   -.580278412E-06    .756479538E-12    .000000000E+00

A POSTERIORI VARIANCE OF UNIT WEIGHT: .300662E-14  DET: .108760E+29

RMS POST FIT RESIDUAL  .055   MICROSECONDS,   16.44 METERS

DOPPLER RESIDUALS USING 10271 POINTS: AVG  .03020 ,    SD  .0815 M/S
```

Figure 5. A MXCKMO summary file printout.

A summary file is output, too. A sample printout is shown in Figure 5. It contains the following items:

- Coefficients of the polynomial clock model and its reference time.
- Mean and standard deviation of pseudorange and Doppler residuals as a bulk.
- Mean and standard deviation of pseudorange residuals, itemized per SV. A certain SV can thus be rejected from a later computation, based on these estimators.
- Epoch when a new ephemeris set was used for the first time, for a given SV, as explained in 4.c. This allows the

user to correlate certain noises with those changes in ephemeris.

C. LONG TERM DETERMINISTIC EFFECTS

Two major deterministic effects, among those mentioned in V.A.2, have been analyzed: temperature changes and transient regimes. Both of them have the same origin: the variations of the temperature in the oscillator. But they affect the operational characteristics of the receiver in different ways. Both of them affect the frequency stability of the clock, in the range of hours. To correlate frequency variations with changes in temperature and warm-up times shows the effect. Unfortunately, the experiments were done under conditions that can hardly be considered as laboratory-like. This is not a major limitation, though. The MX4200 is not a high-performance device. Each particular oscillator is likely to have different characteristics. At least, this is the case for the two receivers tested here. Some trends and ranges can be inferred from the results of these tests, although generalization of the results to all the receivers belonging to the same family is not warranted from this sample of two.

1. Transient regimes

An observation session was held on June 18th, 1991 (day 169) under the following circumstances:

- Receiver model 707361-803, SN 2611, and antenna model 819760-801, SN 0391. Hereafter, this set will be considered as 'receiver 2'.

- TR on, static mode.
- The receiver was off at least 24 hours before the session.
- Data were logged between 16.00 PST (23.00 GMT) and 19.30 PST (02.30, June 19th, GMT) at one second rate.
- Between 3 and 5 SV's were tracked along the session.
- The receiver was inside a small building whose door was opened and closed several times during the session. Short term temperature changes, up to two degrees, can be estimated.

A linear model of the clock offset was generated, using MXCKMO. Doppler residuals, off that model, were extracted. The uppermost part of Figure 6 shows the residuals plotted against time. Residuals off a linear model allows estimating, at a glance, the length of the transient regime. Doppler residuals in fact represent the frequency deviation off the modeled frequency offset.

A transient regime shows up prominently within the two first hours. The jagging in the curve could be due to short term temperature variations in the room. Its effect in the frequency offset will be seen in the following paragraph.

As a matter of generality, a second example is shown here. The observation session was held on April 26th, 1991 (day 116), as follows:

- Receiver model 707361-803, SN 1780, and antenna model 818766-801, SN 0391. This set will be considered as 'receiver 1' hereafter.
- Firmware version D011 was still installed. Thus, TR option was not available.
- Receiver was off at least 24 hours before the experiment.

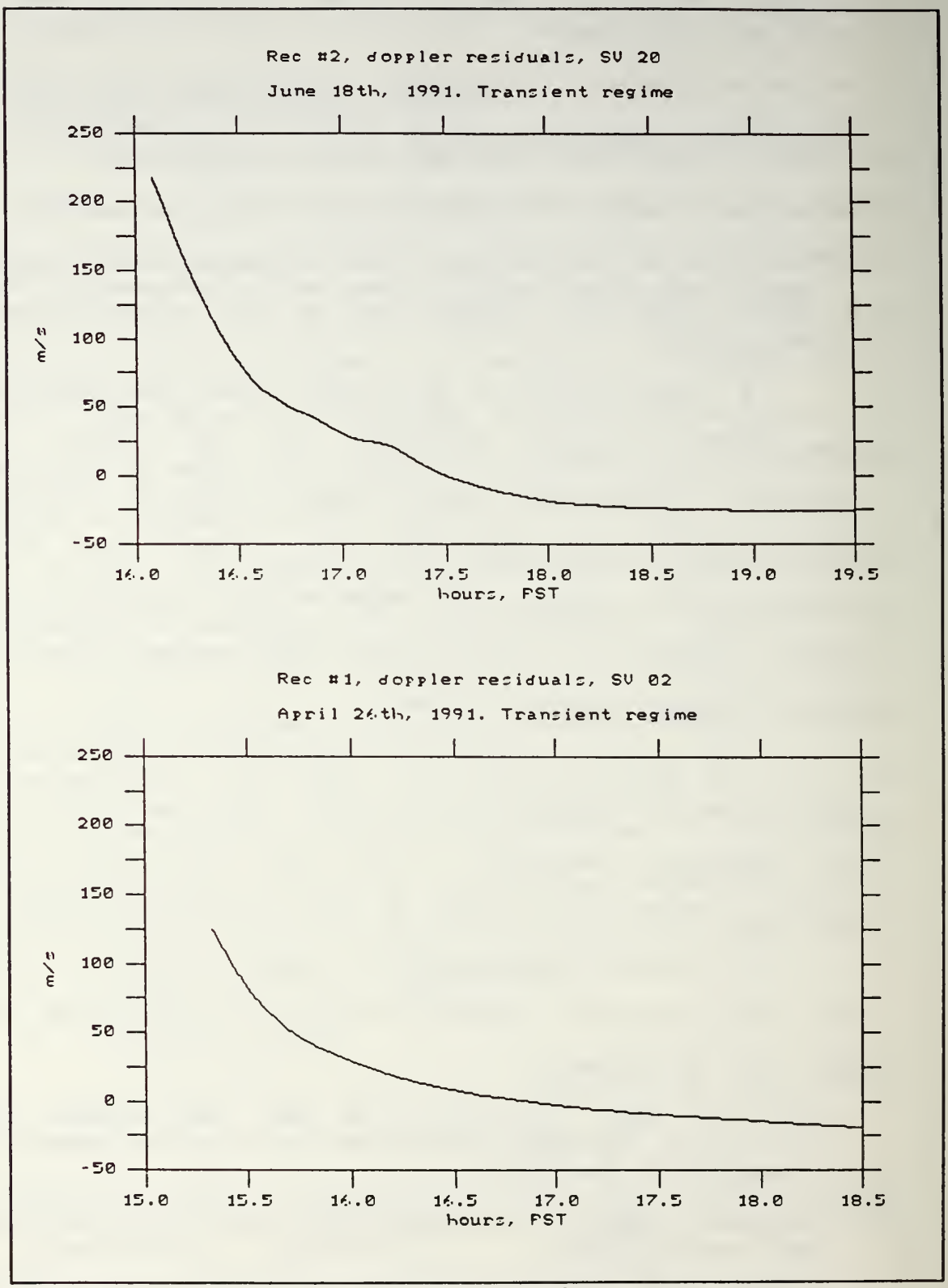

Figure 6. Transient regime in receivers 2 and 1

- Data were logged between 15.00 PST (22.00 GMT) and 18.30 PST (01.30, April 27th, GMT) at 60 seconds rate.
- Four to six satellites were tracked.
- It is presumed to have been exposed to a fairly stable ambient temperature.

The temperature variation, in this case, is estimated to be even less than before. The receiver was inside a fairly well insulated room. An external heat source (TI 4100 GPS receiver) was present in the room. No major air exchange, in a short period, happened.

The same process as above was followed, and the Doppler residuals are shown at the bottom of Figure 6. A transient regime comparable to the one above can be seen during the first two hours. Different ambient temperatures between sessions must count for the initial difference in the size of the residuals. Different performances in both oscillators should be expected, too.

2. Temperature effects

This is a major issue in the performance of the receiver. It was recognized in trying to model a long term data set. Figure 7 shows the Doppler residuals off a linear model generated using the data between 18 and 34 hours. It shows a well developed diurnal pattern. One first thinks of the temperature as its cause. To confirm it, a thermal shock experiment was conducted lasting six hours.

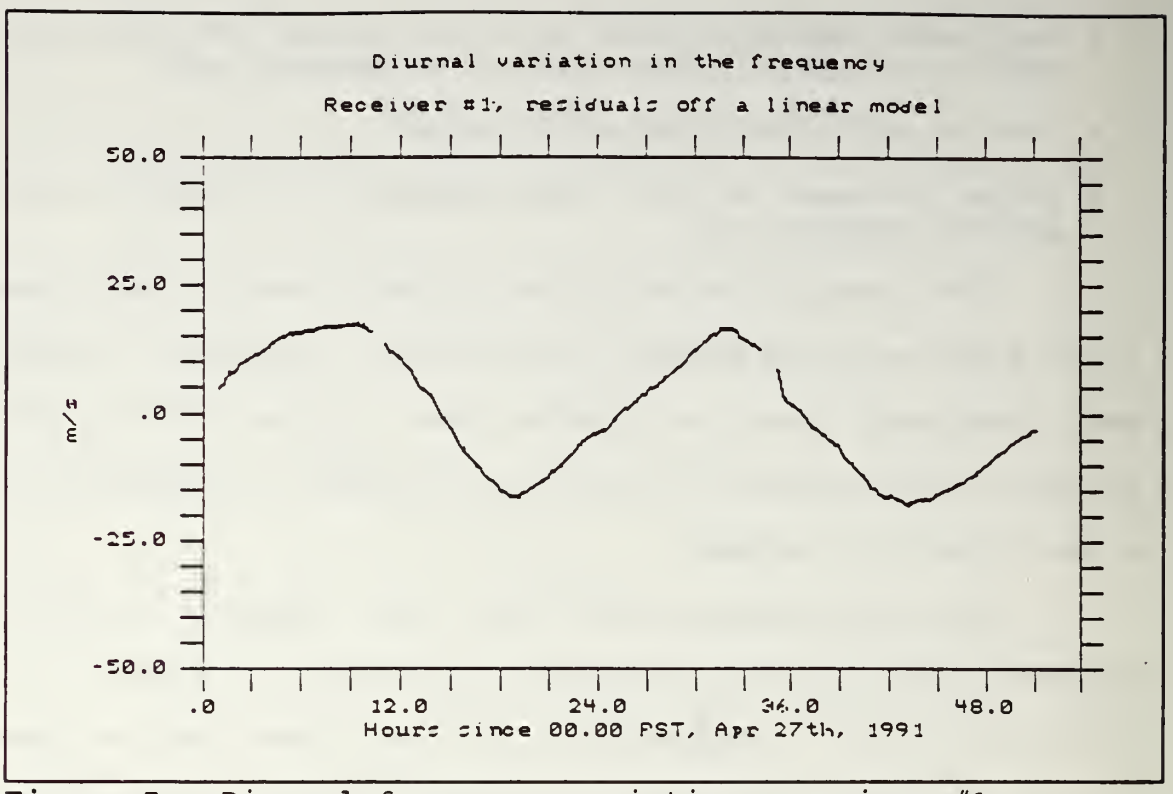

Figure 7. Diurnal frequency variation, receiver #1

At a first stage, receivers 1 and 2 were set to log data, at ambient temperature, for two hours. Transient regimes were avoided by turning the receivers on days ahead. Temperature was recorded with a meteorologic thermograph. Its readings were tested against a calibrated mercury thermometer. An agreement was found, within the resolution of the graph.

In a second stage, both receivers, thermograph and mercury thermometer were put inside a refrigerator. It was turned on several hours in advance. The lid was sealed with foam to prevent heat exchange. This stage lasted for two more hours. Then, all the equipment was removed from the refrigerator. The ambient temperature in the room was close to

30 centigrade. Two more hours of data were collected, so the receivers could reach a steady state.

Data logged every six seconds were used to get a linear model of the clock offset in both receivers. Doppler residuals off their models are plotted in Figure 8, along with temperature. A certain thermal inertia should be expected in the thermograph. It was in fact observed in the third stage of the experiment. Nonetheless, the uncertainty in the recorded temperature should be small, compared to the differential between the receiver's external case and the oscillator.

The difference in patterns shown by the receivers, might well be an effect of an uneven heat exchange. Receiver 2 had to be placed on top of the receiver 1, because not enough room was available. When they were removed from the refrigerator, receiver 1 was warmer, to the touch, than receiver 2. There was another problem with this experiment: two hours in the refrigerator was not enough for the receivers to reach a steady state.

A net effect of the temperature on the frequency is evident now. In an attempt to quantify the effect of the temperature, a new experiment was conducted on August 11th. Both receivers and temperature sensors were left a whole night inside the refrigerator. This time, receiver 2 was below the receiver 1, with about an inch spacing between them.

After one and a half hours of logging data, all the hardware was removed from the refrigerator. They were left at

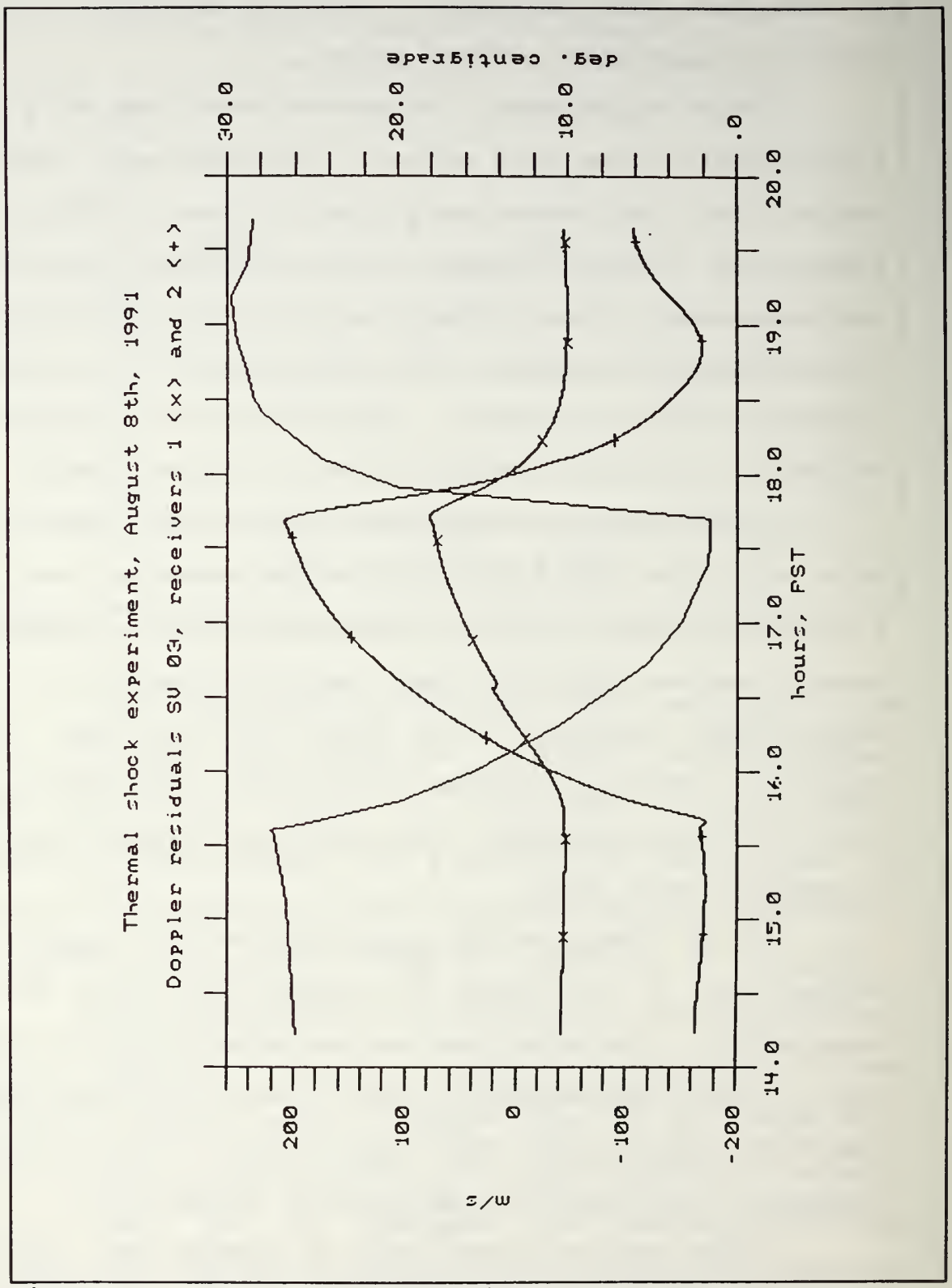

Figure 8. Thermal shock experiment, 08.08.91

ambient temperature for two and a half more hours. Figure 9 is a plot of the Doppler residuals, from a linear model, and recorded temperature. In this case the steady state was reached, both inside and outside the refrigerator. Receiver 2 shows a slightly smaller variation in frequency. This can be due to either different thermal constant, or different rate of heat exchange inside the refrigerator. The crystal oscillators are very likely to have different thermal constants; they are not thought to be subject to very stringent specifications due to the low price of the receiver.

The measured variation in frequency and temperature for receiver 2 leads to a thermal constant of 16.3 m/s/degree in the second test, while a value of 14.9 m/s/degree was obtained in the first experiment, for the same receiver. Steady state was not reached then. These results are in good agreement if some adjustment is allowed accounting for this. Data for receiver 1 in the first experiment cannot be considered valid. A thermal constant of 18.9 m/s/degree was obtained in the second experiment for this receiver.

As a conclusion, the thermal dependence of the receiver clock can be estimated to be somewhere between 15 and 20 meters per second per degree centigrade. This is, between 0.5 and 0.7 hertz per degree centigrade, relative to the nominal frequency, 10.23 Mhz.

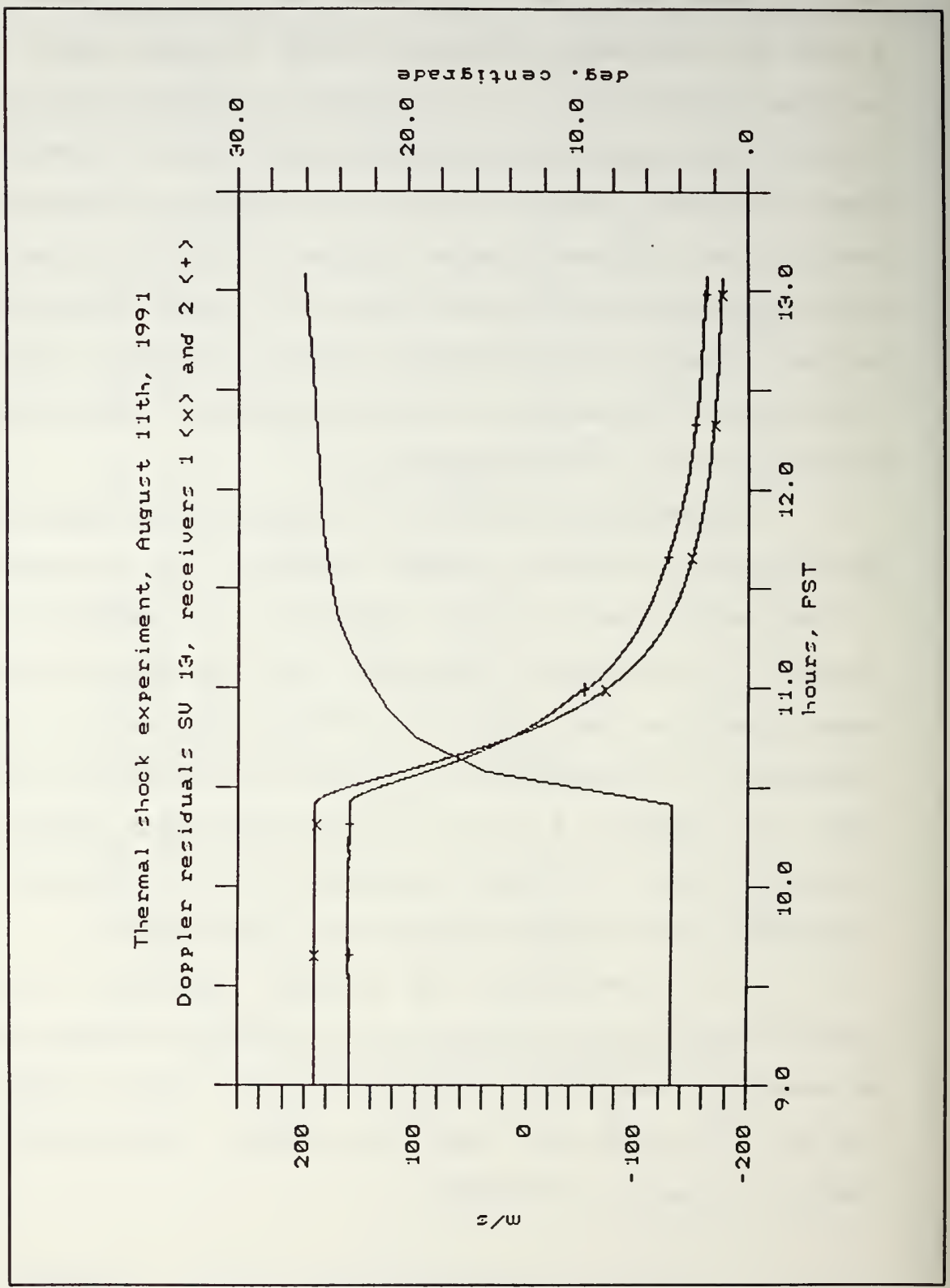

Figure 9. Thermal shock, 08.11.91

VI. CHARACTERIZATION OF THE CLOCK NOISE

The accuracy of a clock can be expressed as the combination of a deterministic and a random component. Stein [Ref. 12:p. 207] and Allan [Ref. 13:p. 3] state that precision oscillators can be described by

$$x(t) = x_0 + y_0 t + \frac{1}{2} D t^2 + \epsilon(t) \qquad (63)$$

where $x(t)$ is the offset of the clock, relative to the absolute time. The first three terms in eq.(63) are the deterministic component and $\epsilon(t)$ is the random component. x_0 represents the initial clock offset, and is termed synchronization error. y_0 represents the initial fractional frequency offset $\Delta f/f_0$ relative to the nominal frequency. It is known as syntonization error. D is the variation in the fractional frequency error and is known as frequency drift or aging.

The degree to which this second order polynomial successfully models the deterministic component of the receiver oscillator is a function of the specific oscillator type and quality. For quartz crystals, y_0 is affected by the environmental conditions (see V.C.2) and D may not be a

constant. For the case at hand, unless the environmental effects are completely isolated, it is not possible to model the deterministic behavior of the clock. Thus, these effects will mask a great deal of the random noise.

The following is a theoretical discussion of the characterization of the random component of the clock offset. This background makes it possible to address the problem of characterizing the noise in the MX4200 receiver.

A. MEASURING THE FREQUENCY STABILITY IN THE TIME DOMAIN

Assume an oscillator generates a voltage signal:

$$\begin{aligned} V(t) &= V_0 \sin\Phi(t) \\ &= V_0 \sin(2\pi f_0 t + \phi(t)) \end{aligned} \tag{64}$$

Here f_0 is the nominal frequency and $\phi(t)$ is the residual phase. This residual phase accumulates the effect of the instantaneous deviation of the actual frequency $f(t)$ from f_0. Because measuring equipment of infinite bandwidth is not physically feasible, $f(t)$ is not a measurable quantity.

While the instanatneous frequency is not measurable, it is the starting point of the timing analysis. It is defined as

$$\begin{aligned} f &= \frac{1}{2\pi}\frac{d\Phi(t)}{dt} \\ &= f_0 + \frac{1}{2\pi}\frac{d\phi(t)}{dt} \end{aligned} \tag{65}$$

Because the deviation from f_0 can be very small, a fractional frequency offset has been defined as

$$y(t) = \frac{f(t) - f_0}{f_0} = \frac{1}{2\pi f_0} \frac{d\phi(t)}{dt} \tag{66}$$

It has the added advantage that it makes the analysis of the frequency fluctuations independent of any scaling factor between the oscillator and the particular circuit where the measurements are being taken.

Integrating eq.(66) yields the instantaneous clock offset:

$$x(t) = \int_0^t y(\tau)\, d\tau = \frac{\phi(t) - \phi(0)}{2\pi f_0} \tag{67}$$

When the signal is sampled at discrete intervals, an average or mean fractional frequency offset at epoch t_k can be defined. This is,

$$\bar{y}_k = \frac{1}{\tau} \int_{t_k}^{t_k+\tau} y(t)\, dt \tag{68}$$

where τ is the sampling interval.

Then, from eq.(67)

$$\bar{y}_k = \frac{x(t_k+\tau) - x(t_k)}{\tau} \tag{69}$$

1. The Allan variance

Certain noise processes in oscillators have a standard deviation that does not converge as $N \to \infty$, i.e., the fractional frequency offset grows unbounded as the size of the data set increases [Ref. 12:p. 201]. Then, the standard deviation is not well-suited for long term analysis. This severely limits its applicability for characterizing a clock behavior. The long term stability is in fact what determines the clock performance as a time keeper.

To deal with this problem, the IEEE recommended the two-sample, no dead time, variance of the mean frequency offset, as a better defined descriptor [Ref. 13:p. 4]. It is known as the Allan variance:

$$\sigma_y^2(\tau) = \langle \sigma_y^2(2,\tau,\tau) \rangle = \left\langle \frac{1}{2} (\bar{y}_{k+1} - \bar{y}_k)^2 \right\rangle \qquad (70)$$

It has been shown to be well defined for all the major noise processes found in an oscillator [Ref. 12:p. 201].

Equations (69) and (70) allow the computation of the Allan variance, based on measured time offsets:

$$\sigma_y^2(\tau) = \frac{1}{2\tau^2} \left\langle [x(t+2\tau) - 2x(t+\tau) + x(t)]^2 \right\rangle \qquad (71)$$

Here the averaging extends to an infinite time. For N discrete time readings, a good estimate of the Allan variance is:

$$\tilde{\sigma}_y^2(\tau) = \frac{1}{2(N-2)\tau^2} \sum_{k=1}^{N-2} [x(t_k+2\tau) - 2x(t_k+\tau) + x(t_k)]^2 \qquad (72)$$

Each pair $x(t_k)$, $x(t_{k+1})$ defines a single average fractional frequency offset in the interval $(t_k, t_k+\tau)$.

Because no dead time exists between measurements, it is possible to define different sampling intervals to be integer multiples of an initial τ_0. Therefore

$$\tilde{\sigma}_y^2(m\tau) = \frac{1}{2(N-2m)m^2\tau_0^2} \sum_{k=1}^{N-2m} [x(t_k+2m\tau_0) - 2x(t_k+m\tau_0) + x(t_k)]^2 \qquad (73)$$

gives a good estimate of the Allan variance for a sampling interval $m\tau_0$.

2. Confidence intervals

Consider a series of time offset measurements x, spaced τ in time. Two consecutive values x_k, x_{k+1} yield a single mean fractional frequency offset $\bar{y}_k$. x_{k+1} and x_{k+2} define $\bar{y}_{k+1}$. Thus, those three consecutive values give a single sample Allan variance.

For the common oscillators, the first difference of the frequency is a normally distributed variable with zero mean [Ref. 12:p. 210]. The square of a normally distributed variable follows a Chi-squared distribution with one degree of freedom.

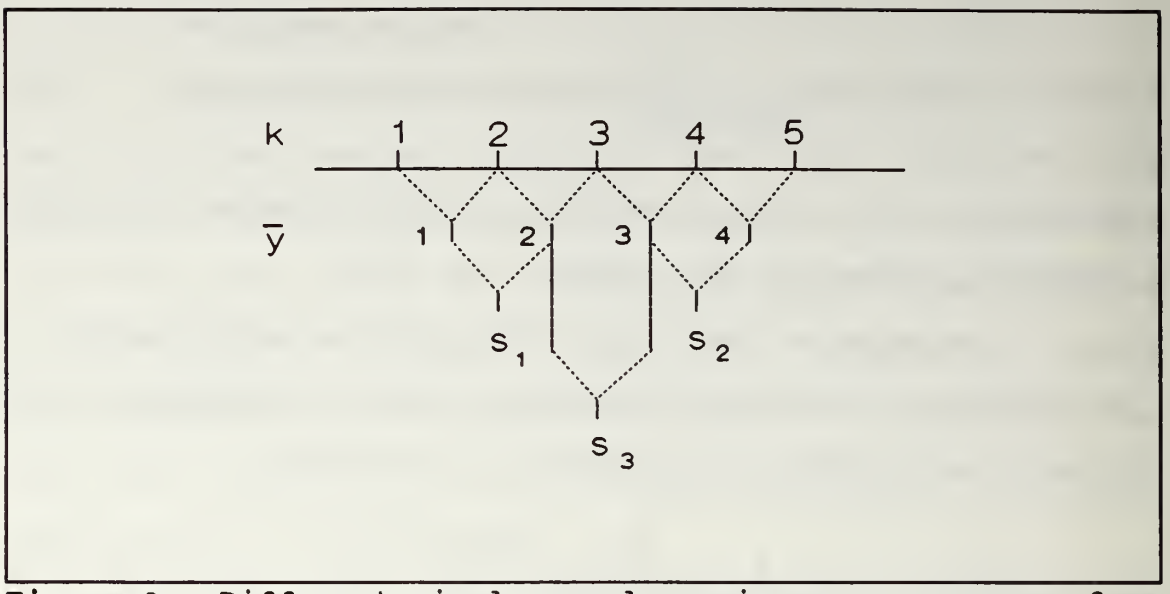

Figure 9.- Different single sample variances, s_1, s_2, s_3, from the same data. k is the clock reading number, and $\bar{y}$ is the mean fractional frequency error corresponding to consecutive clock readings

Consider now the five time offset values shown in Figure 9. From readings 1 to 3 we can get a single sample Allan variance $s_1^2(\tau)$; from readings 3 to 5 a new sample Allan variance $s_2^2(\tau)$ is obtained. In averaging them, a better estimate of the true Allan variance is obtained

$$\bar{\sigma}_y^2(\tau) = \frac{1}{2}(s_1^2 + s_2^2) \qquad (74)$$

which has a tighter confidence interval. Now, $\bar{\sigma}_y^2(\tau)$, as a sum of two squared, independent, normally distributed variables, follows a Chi-squared distribution with two degrees of freedom.

For a better exploitation of the data, a new sample variance $s_3^2(\tau)$ can be obtained as:

$$s_3^2(y) = \frac{1}{2}(\bar{y}_3 - \bar{y}_2)^2 = \frac{1}{2}(x_4 - 2x_3 + x_2) \quad (75)$$

But this sample variance is not independent of the previously computed ones. A better estimate of the true Allan variance is obtained by averaging all three. But this estimate does not follow a Chi-squared distribution with three degrees of freedom.

The actual number of degrees of freedom is a complicated matter, beyond the scope of this work. It basically depends on the underlying noise type, and can take fractional values. Barnes [Ref. 14:p. 10] gives expressions to compute the degrees of freedom as a function of the number of samples, and the sampling interval. Those expressions are reasonably well suited for the five major noise types found in an oscillator.

From the point estimate computed above, an interval estimate of the Allan variance can be obtained as follows:

$$X^2_{\nu,\frac{\alpha}{2}} < \frac{\nu\tilde{\sigma}_y^2(\tau)}{\sigma_y^2(\tau)} < X^2_{\nu,1-\frac{\alpha}{2}} \quad (76)$$

at a confidence level α, for ν degrees of freedom.

As can be seen, the computation of this interval estimate is somewhat complicated. First, it involves determining the number of degrees of freedom. In turn, it implies some assumptions about the kind of noise present in the data, for the given sampling interval. In addition, the number of degrees of freedom is only empirically obtainable for some of the stochastic processes in an oscillator [Ref. 14:p. 7]. Finally, the Chi-squared distribution for a non integer number of degrees of freedom has to be used.

A simpler approach is given by Stein [Ref. 12:p. 213], citing Lesage and Audoin [Ref. 15] and Yoshimura [Ref. 16]. It is based on computing the variance in the estimate of the Allan variance.

For N single time offset values, N-2 sample Allan variances are obtained. Averaging them all, the resulting estimate $\tilde{\sigma}_y^2(\tau)$ will deviate $\Delta(N)$ from the true Allan variance:

$$\tilde{\sigma}_y^2(\tau) = (1+\Delta(N))\,\sigma_y^2 \qquad (77)$$

Here $\Delta(N)$ has mean zero. For N greater than 10, the variance of Δ is approximately given by

$$\sigma^2(\Delta) \approx \frac{C_\alpha}{N} \qquad (78)$$

where C_α, again, depends on the kind of noise in the process. Thus, the true Allan variance, at a 67% confidence level, can be approximated by

$$\tilde{\sigma}_y(\tau)\left(1-\sqrt{\frac{C_\alpha}{N}}\right) < \sigma_y(\tau) < \tilde{\sigma}_y(\tau)\left(1+\sqrt{\frac{C_\alpha}{N}}\right) \qquad (79)$$

Table 4 shows the value of C_α for the five major noise processes in an oscillator.

TABLE 4. VALUES OF C_α FOR THE MAJOR NOISE TYPES

Noise Type	α	C_α
White Phase	2	3.88
Flicker phase	1	3.88
White frequency	0	2.99
Flicker frequency	-1	2.31
Random walk frequency	-2	2.25

B. STOCHASTIC PROCESSES IN AN OSCILLATOR

The stochastic clock noise is often represented, in the frequency domain, as

$$S_y(f) = \sum_{\alpha=-\infty}^{\infty} h_\alpha f^\alpha \qquad (80)$$

where f is the Fourier frequency. $S_y(f)$ is the one sided power spectral density of the phase fluctuations, and h_α is the amplitude of the α-th term.

Five major stochastic processes have been described in precision oscillators [Ref. 13:p. 4][Ref. 12:p. 204]. They correspond to the terms -2 to 2 and named as follows:

- Random walk noise, frequency modulation (FM). α=-2.
- Flicker noise, FM. α=-1.
- White noise, FM. α=0.
- Flicker noise, phase modulation (PM). α=1.
- White noise, PM. α=2.

Those five stochastic processes also can be described in the time domain. A plot of the square root of the Allan variance, in a log/log scale, typically looks as shown in Figure 10. The sharp corners between segments is a simplification for discussion purposes.

A different kind of noise dominates in each of these regions. The slope of the corresponding segment, μ is given below:

- I.- White PM and Flicker PM, $\mu\approx$-1.
- II.- White PM, μ=-1/2.
- III.- Flicker FM, μ=0.
- IV.- Random walk FM, μ=+1/2.

This pictorial description is very useful in characterizing the noise in a frequency standard.

Region III shows no dependence on the sampling interval. It is known as the Flicker floor. Its physical cause is not fully understood yet. It represents the limit in the frequency stability of a clock, i.e., its accuracy. For a time standard,

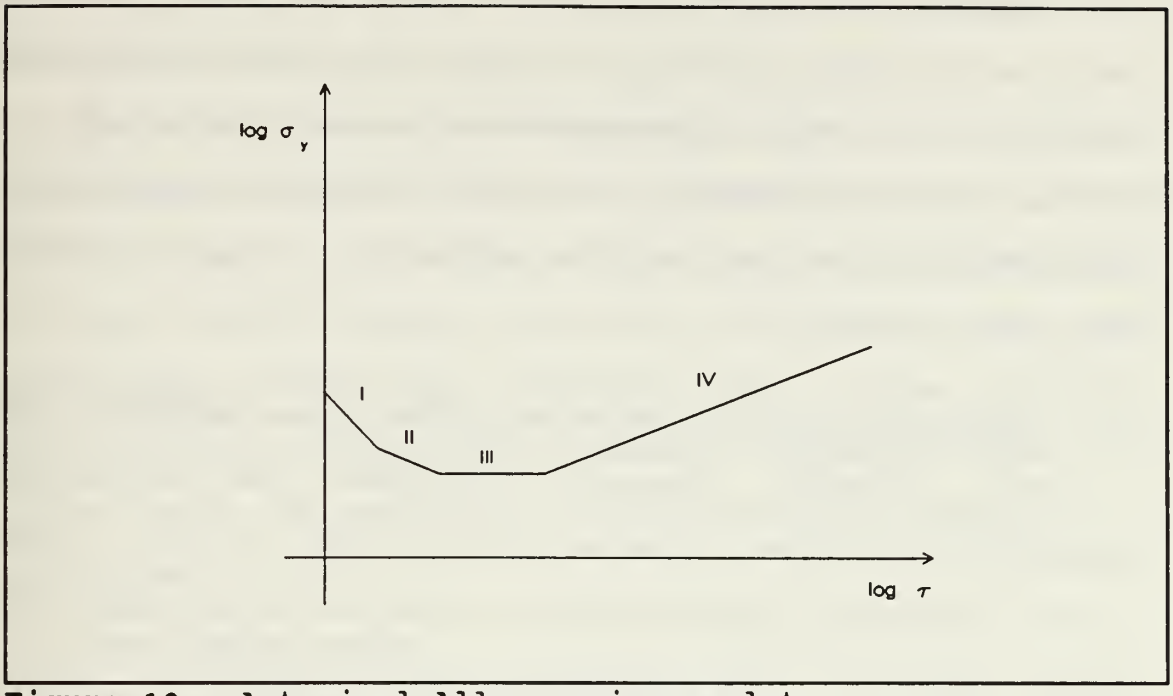

Figure 10.- A typical Allan variance plot

it is desirable to have the flicker floor at the longest sampling interval possible. The best measured frequency stability reported by Hellwig [Ref. 17:p. 566] for passive hydrogen maser resonators locates the Flicker floor at a sampling interval longer than 10^6 seconds.

For crystal oscillators, that Flicker floor can be located somewhere between 10^{-2} and 10^4 seconds. Thus, they are not well suited for a long term time keeping. For short term intervals, they can show a better stability than most atomic resonators, though. That is why both kinds of oscillators are used together to form a time-frequency standard.

Region IV is extremely sensitive to the frequency drift *D* in eq.(63). The clock offset grows at a rate of the square of

the sampling interval if D is not zero. A linear frequency drift would yield a slope μ=1 in region IV. As a deterministic effect, it should be removed from the data beforehand. This is not an easy task because the drift is highly dependent on environmental effects, and its effect is integrated over a very long period.

C. CHARACTERIZATION OF THE NOISE IN THE MX4200 RECEIVER CLOCK

The preceding discussion provides the theoretical background for the analysis of the noise in the receiver clock. The common approach for this analysis is to compute the clock offset at many different epochs, spaced τ. Eq.(63) models this offset as a function of the interval following synchronization. The instantaneous offset $x(t)$ has to be computed as the difference between readings of the clock (under investigation) and a frequency standard. It is assumed that the frequency standard has such a high degree of frequency stability that the effect of its fluctuations on $x(t)$ is negligible.

The GPS SV's provide such a frequency standard, in comparison to a crystal oscillator. The readings of the receiving clock can be compared with this standard by subtracting the true range from the measured range, as was explained in Chapter V. The program MXCKMO already corrects the receiver clock for the major deterministic effects,

including its own model. Then, the output residuals are in fact $\epsilon(t)$ in eq.(63).

Here, the aforementioned assumption about the standard's frequency stability is legitimate. The noise level in the SV clock is several orders of magnitude below the noise in the receiver clock. Several systematic factors in the whole measurement process may introduce noise in the residuals, though. Those in the higher frequency range would mask the actual noise in the clock at short sampling intervals. In particular:

- Pseudorange noise
- Changes in the selected ephemeris
- SA activation
- Loss of lock on the SV

need to be carefully watched. Other long term deterministic effects were discussed in Chapter V. The effect of the temperature on the long term noise will be seen here, too.

1. Analysis tools

a. Program MXALLV

The main analysis tool here is the program MXALLV, listed in Appendix I. It computes the Allan variance of the range residuals following eq.(73). Programs MERGE and MXFXRS act as interfaces between the MXCKMO output and MXALLV.

b. Program MERGE

This program generates a single file with residuals from different satellites. The maximum time a SV can be tracked is about five hours. This is the time the SV is above the observer's horizon. With this program, a single residuals file can be obtained for a longer observation session. It accepts residuals if they are not flagged as anomalous. Once it gets to the end of the file, or when a flag is detected, the program prompts a new input file. Then, it fetches the new file until the last valid epoch in the previous file is found. The difference between residuals of both SV's will be applied to all the residuals in the new file. This allows to get a continuous sequence of residuals from the beginning to the end of the session. Otherwise, discontinuities in that sequence would degrade the Allan variance at short sampling intervals.

c. Program MXFXRS

Gaps may exist in the residuals file that MXCKMO outputs. For the Allan variance to be properly computed, a continuous sequence of samples has to be taken. If the number of missing epochs is small, MXFXRS synthesizes the missing residuals by interpolating between the closest records. This approach is not valid if more than 1% of the data is missing, because it artificially decreases the noise level.

d. Program CONFIN

This program makes it possible to go from the point estimate computed by MXALLV to the interval estimate given in eq.(76). The user selects a confidence level, and the point estimate Allan variance is then displayed. The decision about the boundaries between noise regions, as depicted in Figure 10, is left to the user. The number of degrees of freedom is computed accordingly, using the equations in Barnes [Ref. 14:p. 10]. The parameter α in eq.(76) is being shifted until the probabilities

$$P(X^2_{\nu} > X^2_{\nu,\alpha/2}) = \frac{\alpha}{2} \tag{81}$$

and

$$P(X^2_{\nu} > X^2_{\nu,1-\alpha/2}) = 1 - \frac{\alpha}{2} \tag{82}$$

Then, the interval extremis are found as

$$\sigma_y(\tau)_{\min} = \tilde{\sigma}_y(\tau) \sqrt{\frac{\nu}{X^2_{\nu,\alpha/2}}} \tag{83}$$

$$\sigma_y(\tau)_{\max} = \tilde{\sigma}_y(\tau) \sqrt{\frac{\nu}{X^2_{\nu,1-\alpha/2}}} \tag{84}$$

2. Short term analysis

The effect of the temperature on the clock noise should not be a major problem for short periods. An example is examined here to confirm this. An observation session was held on June 18th, 1991 (day 169), under the following circumstances:

- Receiver 1.
- Time recovery enabled.
- Data logged at 1 s. rate, during 3.3 hours.
- The receiver was inside a fairly well insulated room.
- SA was not activated.

A quadratic clock offset model was fitted to the data. That meant that a constant drift in the clock frequency was assumed. If the clock frequency did in fact have a constant drift, the resulting Allan variance accurately describes the stochastic noise. No temperature record was kept in that session. A constant drift in the frequency might have been due to either a constant rate of change in the temperature, or aging. It does not seem reasonable to expect aging effects for such a short period. If there were any, they would be masked by temperature effects. To assume a linear change in temperature over this period seems to be an over simplification.

The resulting Allan variance is shown in Figure 11. The general shape of the curve matches fairly well with what should be expected. The Flicker floor is located at about one

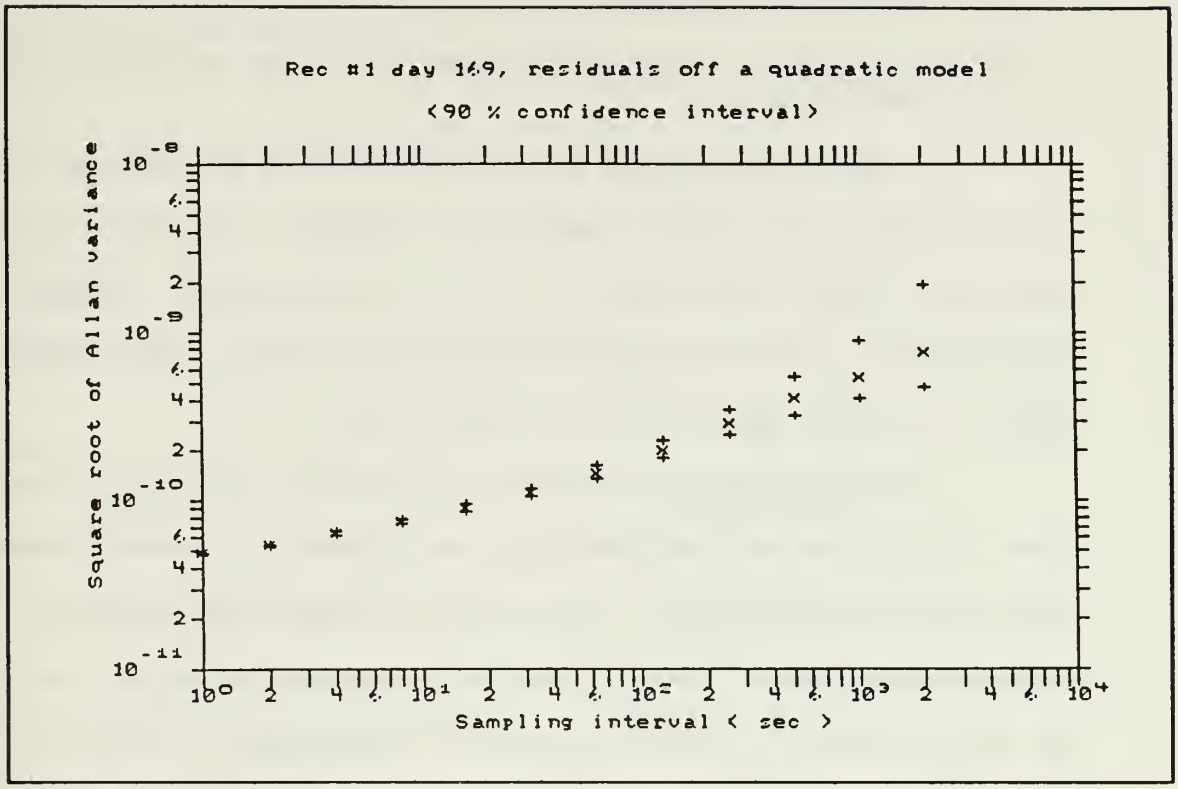
Rec #1 day 149, residuals off a quadratic model
(90 % confidence interval)
Square root of Allan variance
Sampling interval (sec)

Figure 11.- The short term Allan variance in receiver 1

second. In the range 1-20 seconds, both Flicker FM and Random Walk FM noises are present. The last dominates at sampling intervals longer than 20 seconds. There are many crystal oscillators that show a Flicker floor all the way down to the one second sampling interval. Shorter samples could not be taken because one second is the interval between measurement epochs.

Another observation session was held on May 30th, 1991 (day 150), as follows:

- Receiver 2
- Time recovery enabled
- Data logged at 1 second rate, during 40 minutes

- SA was not activated
- Environmental conditions expected to be as stated before for receiver 1.

A quadratic model was fitted to the residuals from SV 6. In this case, the observation session was much shorter, although Allan variance up to one thousand seconds was obtainable. The confidence interval is wider, too. They are plotted in the upper part of Figure 12.

In comparing the results for both receivers, a smaller level of noise was noticed for the number 2. There is also a qualitative difference. The Flicker floor for receiver 2 is somewhere between 1 and 4 seconds sampling interval and white FM noise seems to dominate at the measurement interval, one second. The noise level at this sampling interval, for receiver 2, is about 2/3 the one in receiver 1. It is less than 1/2 for sampling intervals longer than 4 seconds.

To confirm these results, data from a previous observation session were analyzed. They were gathered the day before, under similar circumstances, with receiver 2. The Allan variance of the phase range residuals to SV 6 is plotted at the bottom of Figure 12. A quadratic clock model was removed, too.

In this case, a non-constant linear drift seems to be present in the clock. It could be due to temperature changes. The slope in the tail of the curve is greater than 1/2. That means that deterministic effects are masking the long term

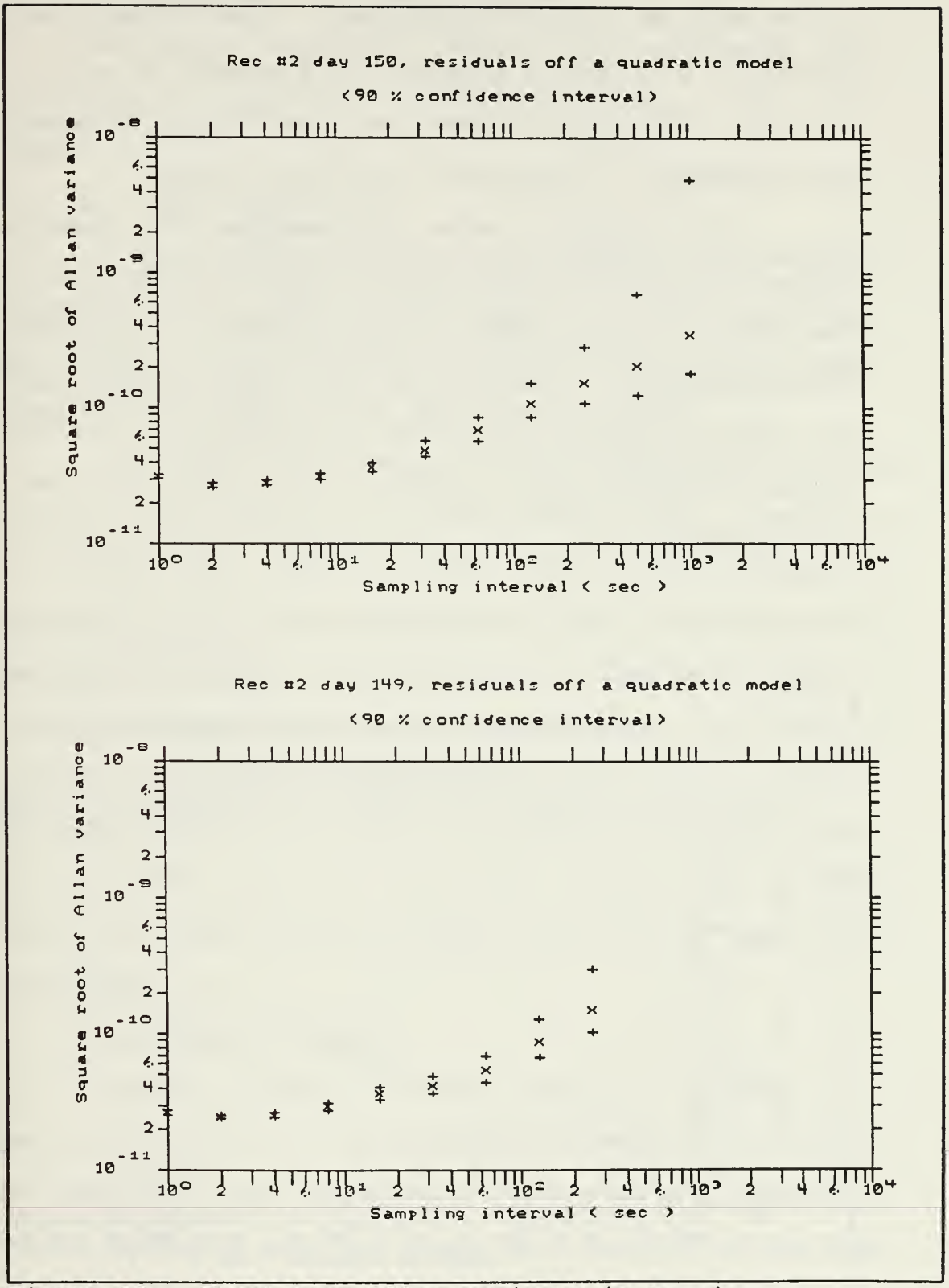

Figure 12.- Short term Allan variance in receiver 2

random walk FM noise. Nevertheless, those effects should be negligible at sampling intervals of a hundred seconds or less. In fact, the upper and lower parts of Figure 12 show a very good agreement in the short term noise levels.

In contrast, noise for session 150, receiver 1, (Figure 13) shows the same characteristics as we found before. The set up was the same as for receiver 2. The results are very consistent, no matter what the length of the session was (40 minutes versus 3 hours and 20 minutes). In conclusion, a higher noise level in receiver 1, on a short term basis, has been measured.

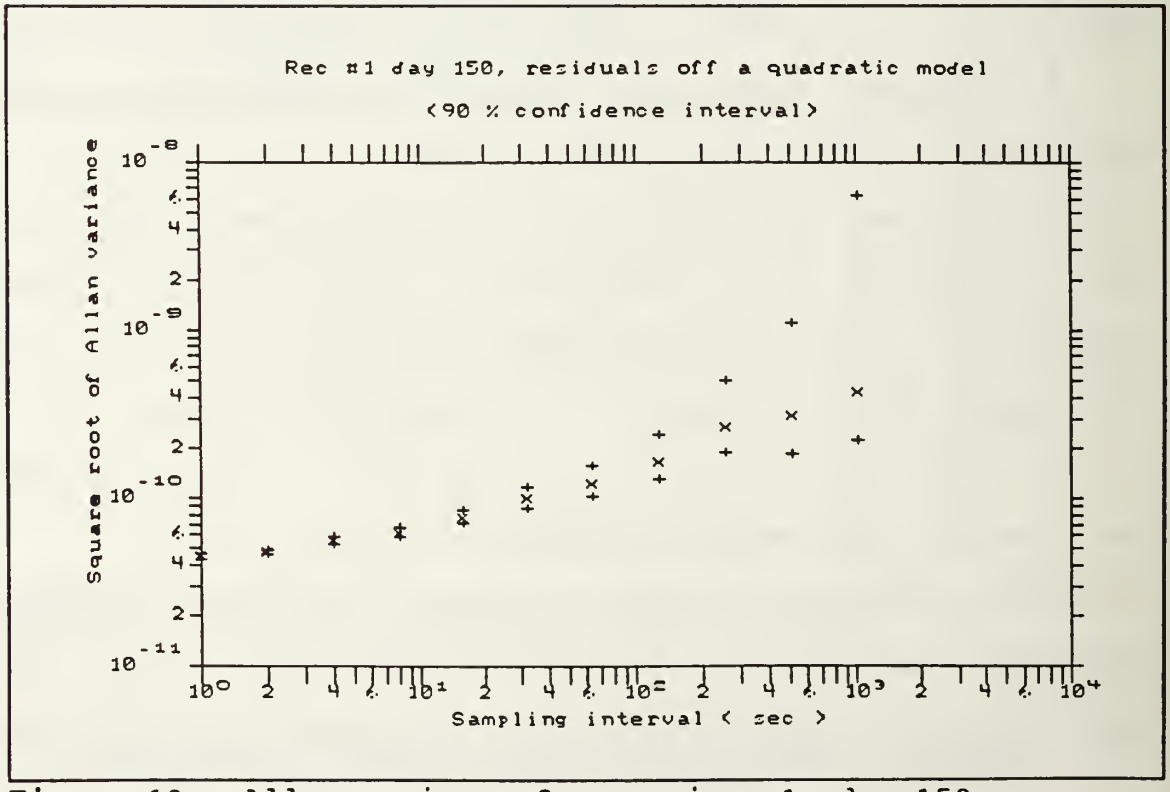
Rec #1 day 150, residuals off a quadratic model
(90 % confidence interval)
Square root of Allan variance
Sampling interval (sec)

Figure 13.- Allan variance for receiver 1, day 150.

3. High frequency systematic effects

Four major systematic effects were mentioned above that should be carefully watched in getting the Allan variance.

a. Pseudorange noise

The residuals that the clock model program outputs are computed using phase derived ranges. At short intervals, higher levels of noise should be expected using pseudoranges, because of the nature of the measurement process.

A slight modification in the MXCKMO program was done to get the residuals from the pseudoranges, instead of phase ranges. The resulting Allan variance is plotted in Figure 14 as (x). The corresponding Allan variance of the phase range residuals is plotted as (+). The noise here is dominated by processing noise in the correlator. Its level is more than one order of magnitude at the shorter sampling times. Both of them converge for sampling intervals larger than 100 s. This would be a good time constant for the CODE variable in eq.(42) to be filtered, before being input into the navigator.

b. Ephemeris changes

This is not a trivial question, sometimes not properly accounted for. The parameters needed for the true range computation are contained in the broadcast ephemeris. Different ephemeris sets are chosen as a function of the time

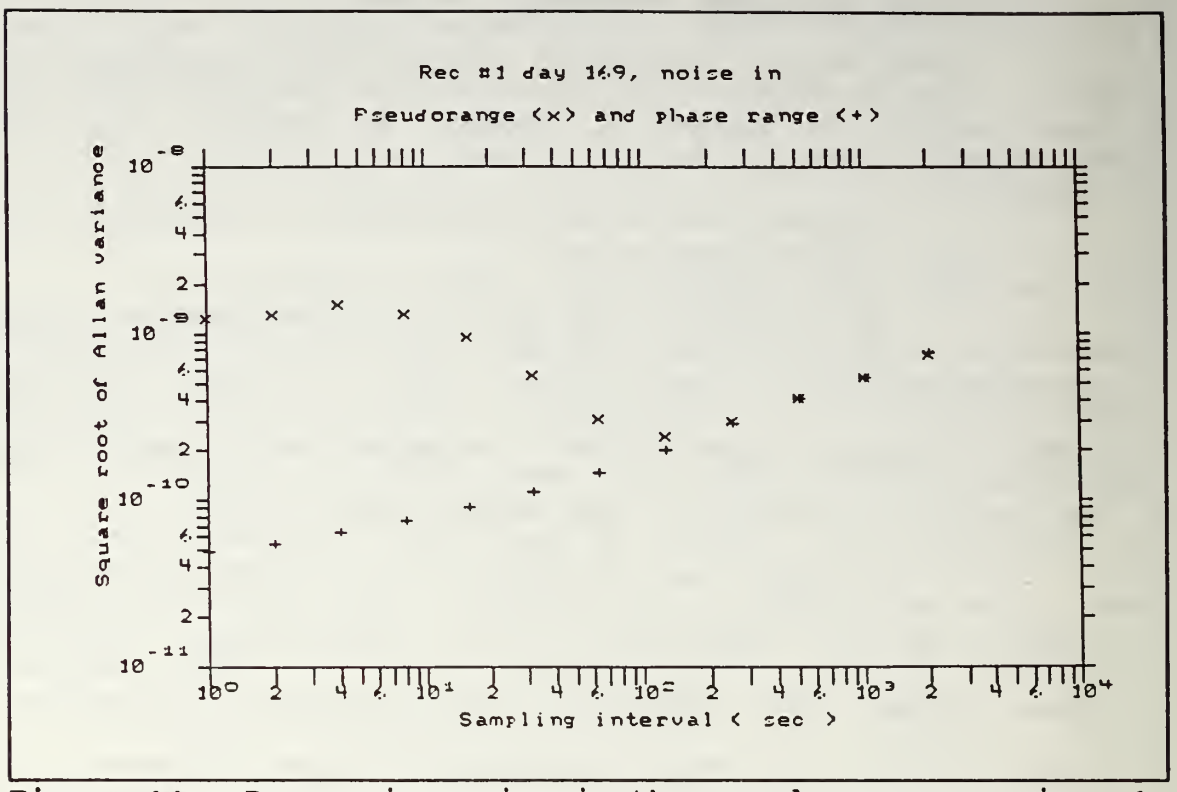

Figure 14.- Processing noise in the pseudorange, receiver 1

difference between the ephemeris epoch and the measurement time. The computed range to the SV, then, shows discontinuities, whenever the program switches from one ephemeris set to another.

This has a noticeable effect on the high frequency noise, if not properly filtered. The program MXCKMO biases the OMC's by those discontinuities, so the resulting true range is smoothed. An estimate of the effect of leaving these jumps in follows.

Assume a discontinuity δ in the OMC exists between epochs $j+1$ and $j+2$, as shown in Figure 15. Two sample variances will be affected: $(j,\ j+2)$ and $(j+1,\ j+3)$. The OMC

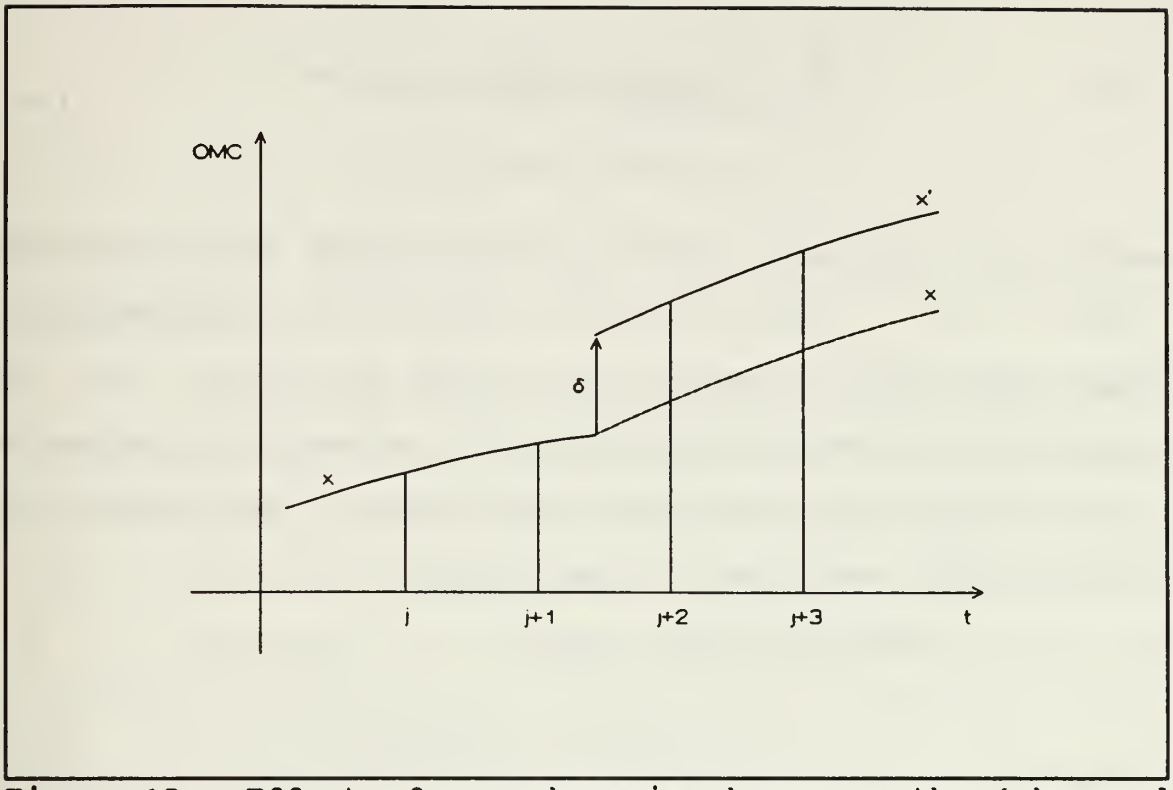

Figure 15.- Effect of an ephemeris change on the 'observed minus computed' (OMC) range.

is represented by x before the discontinuity, x' after it. Following eq.(72), let $\sigma_y'^2$ be the Allan variance corresponding to these OMC's:

$$\sigma'^2_y(\tau_0) = \frac{1}{2\tau_0^2(N-2)}\Big[\sum_{k=1}^{j-1}(x_{k+2}-2x_{k+1}+x_k)^2 + (x_{j+2}+\delta-2x_{j+1}+x_j)^2 + (x_{j+3}+\delta-2(x_{j+2}+\delta)+x_{j+1})^2 + \sum_{k=j+2}^{N-2}(x_{k+2}+\delta-2(x_{k+1}+\delta)+x_k+\delta)^2\Big] \quad (85)$$

All the δ's in the last term cancel. Gathering terms in x, eq.(85) becomes

$$\sigma'^{2}_{y}(\tau_0) = \frac{1}{2(N-2)\tau_0^2}\left[\sum_{k=1}^{N-2}(x_{k+2}-2x_{k+1}+x_k)^2\right. \tag{86}$$

$$\left. + 2\delta^2 + 2\delta(x_{j+3}-x_{j+2}-x_{j+1}+x_j)\right]$$

Let σ_y^2 be the Allan variance corresponding to the unbiased OMC's, i.e., to the x's before and after the discontinuity. The first term in eq.(86) is in fact this value. The last parenthesis in eq.(86) must be small, compared to δ. Values of δ larger than ten meters have been observed. The contribution of the last term, thus, is negligible.

Eq.(86), then, becomes

$$\sigma'^{2}_{y}(\tau_0) \approx \sigma_y^2(\tau_0) + \frac{1}{(N-2)\tau_0^2}\delta^2 \tag{87}$$

for a single discontinuity. If M discontinuities exist in the data, each one contributes a new term. It should be pointed out that changes in ephemeris can happen once in an hour for a given SV. Thus,

$$\sigma'^{2}_{y} \approx \sigma_y^2 + \frac{1}{(N-2)\tau_0^2}\sum_{i=1}^{M}\delta_i^2 \tag{88}$$

Their effect, at a sampling interval $m\tau_0$ will be

$$\sigma'_y{}^2(m\tau_0) \approx \sigma_y{}^2(m\tau_0) + \frac{1}{(N-2m)m^2\tau_0{}^2}\sum_{i=1}^{M}\delta_i{}^2 \qquad (89)$$

although as m grows, the last term in eq.(86) may become comparable to δ^2.

Figure 16 shows the effect of changing ephemeris on the Allan variance, at short time intervals. The points marked (x) correspond to the Allan variance of the data if those jumps are not removed. This is, σ_y' in eq.(89). Points marked as (+) correspond to σ_y, i.e., the Allan variance of the residuals, once filtered by discontinuities in OMC. It is, in fact, the same Allan variance shown in Figure 11. Residuals from SV 20 were used there. A change in ephemeris occurred at epoch 262814. Its effect on the computed range had a magnitude of -7.14 meters. Let us check eq.(88) against the values shown in Figure 16. In this case, N was 12053, and M was 1. For a one second interval

$$\frac{\delta^2}{\tau_0{}^2(N-2m)} = \frac{(-7.14)^2}{(3\cdot 10^8)^2\cdot 12051} = 4.7\cdot 10^{-20} \qquad (90)$$

where the increment in computed range has been scaled to time. From the plots in Figure 16 we get:

$$\sigma'_y{}^2(\tau_0) - \sigma_y{}^2(\tau_0) = (2.2\cdot 10^{-10})^2 - (0.49\cdot 10^{-10})^2 = 4.59\cdot 10^{-20} \qquad (91)$$

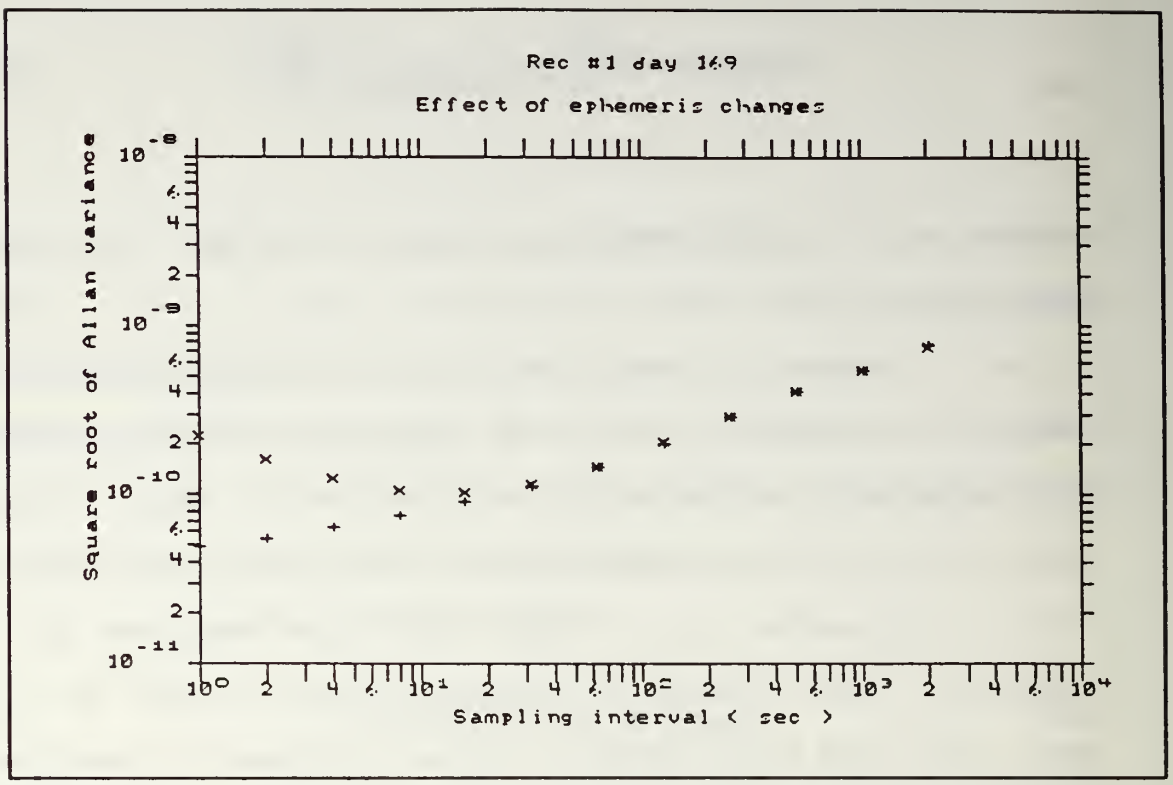

Figure 16.- The effect of ephemeris changes in the short term Allan variance

For a different sampling interval, the agreement is not as good. If $m = 5$

$$\frac{(-7.14)^2}{(12053-2\cdot 5)\cdot 5^2\cdot (3\cdot 10^8)^2}=0.19\cdot 10^{-20} \qquad \textbf{(92)}$$

whereas from the plot

$$\sigma'^2_y(5)-\sigma^2_y(5)=0.26\cdot 10^{-20} \qquad \textbf{(93)}$$

As the sampling interval increases, the last term in eq.(86) may effectively increase, compared to δ^2. It produces slightly different results.

c. Temporary loss of lock and cycle slips

A tracked SV can be temporarily lost. At reacquisition, a different bias is introduced in the phase-derived range. This bias is on the order of the noise in the pseudorange, i.e., several meters. Its effect on the Allan variance is expected to be of the same order as the changes in ephemeris. Nothing can be done to correct for the new bias. But the data should be carefully watched to avoid computations on residuals from a SV that was temporarily lost. The program MXCKMO can detect spikes in the OMC larger than about a meter. Thus, a reasonably quantity of them are flagged as bad records. The Allan variance routine will not accept a residuals file with those kinds of records in it.

This problem is especially harmful when the logging interval is longer than one second. Otherwise, the lock loss is easily detected if measurements to that SV are missing for a few seconds.

Cycle slips have not been detected, and it appears to be very unlikely. Their size is in the order of decimeters, so it would be hard to detect them. Their effect on the Allan variance would not be much of a problem, because they are so infrequent.

d. Selective Availability activation

Not too much is known about the way SA is implemented. Higher level of noise, both in CA code and in L1 frequency should be expected. Whether that level is above or below the receiver noise could not be checked.

SA was activated on July 2nd, 1991 [Ref. 18]. Several pieces of data were logged after that. The observed noise in the phase range residuals, as depicted by the Allan variance, stayed at the same level as before.

4. Long term analysis

Long term here refers to observation sessions lasting more than a complete pass of a satellite. The analysis has to be performed on a sequence of residuals of more than one SV. Residuals from different SV's are biased to those of the earliest one, as explained in VI.C.1.b. So, the entire sequence is internally consistent.

Plenty of data were gathered in long term sessions. Unfortunately, the effect of the temperature changes contaminates most of those data sets. A few more tests were done attempting to thermally isolate the receivers. Sometimes the receivers were taken inside a refrigerator, in an attempt to keep the temperature unchanged. Comparisons between inside and ambient temperatures were done. The temperature inside the refrigerator followed the main ambient trend, by a factor of one half. In addition, acceleration effects, due to the

compressor cycle, added an extra complication. No significant result was obtained by this procedure.

A second approach was followed. Receivers were left at ambient temperature, in a closed room, with an external heat source. A temperature record was used to estimate a period of constant rate of change on temperature. A linear drift in the frequency should be expected then. This is, D in eq.(63) should be

$$D=D(t)=D_0+\frac{D_1}{3}t \tag{94}$$

so eq.(63) becomes

$$x(t)=x_0+y_0t+\frac{1}{2}D_0t^2+\frac{1}{6}D_1t^3+\epsilon(t) \tag{95}$$

Thus, a cubic model, rather than quadratic, would be needed to remove this deterministic effect. This was done on data from day 221 (August 10th, 1991). Receiver 2 was logging data for 24 hours, at a 15 second rate. A linear model was first computed for the whole session. A plot of the Doppler residuals from that model is shown in Figure 17. From that plot, a linear frequency drift can be estimated between between 00.00 PST and 09.00 PST, August 10th. It matched the temperature records.

Data were then processed between those epochs. This time, a cubic model was generated. The resulting Allan

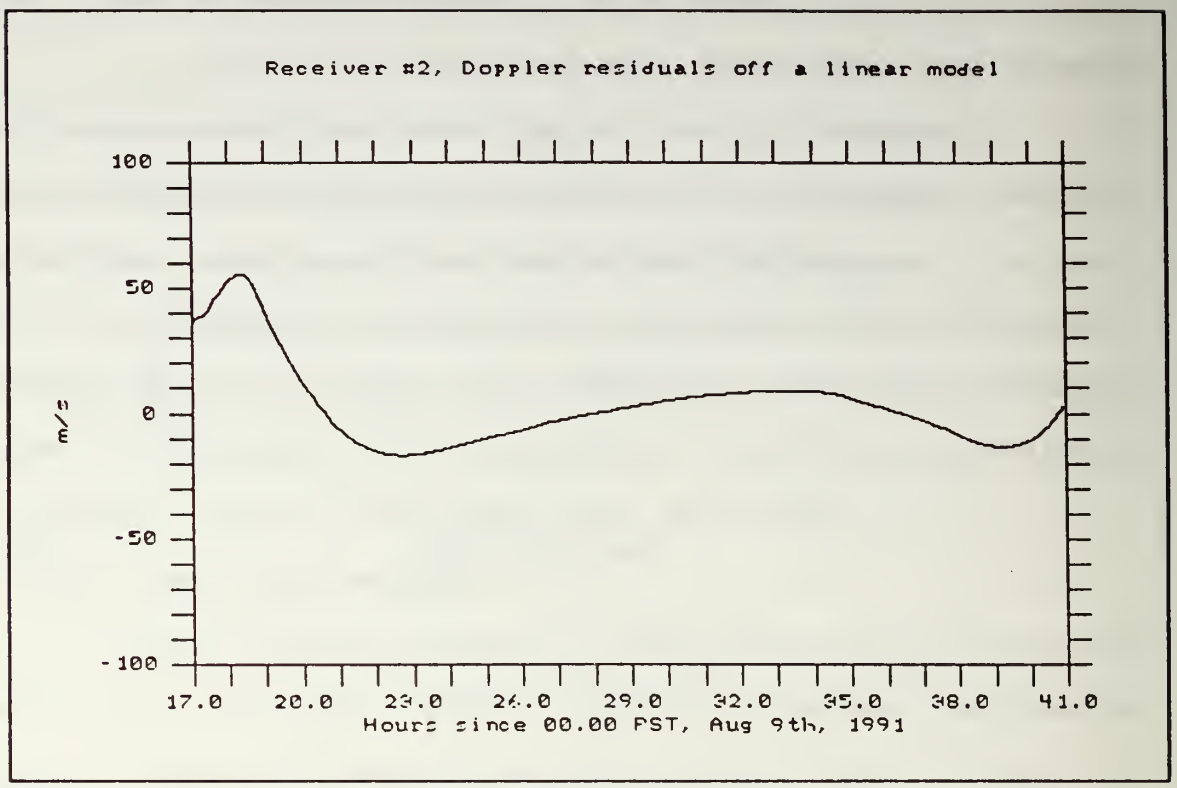

Figure 17.- Doppler residuals off a linear model. Receiver 2, day 221

variance is shown in Figure 18. The slope in the curve (1/2) corresponds to the expected random walk FM noise. Systematic effects seem to have been removed. The agreement with plots in Figure 12 in the overlap region is good.

A comparable test for receiver 1 was not possible. Earlier data were reviewed. A linear fit to data from day 117 showed an almost constant frequency drift between 20.00 PST, April 27th, and 07.00 PST April 28th (Figure 19). No temperature data were available then. Data were reprocessed for that interval, and a quadratic clock offset model generated. The Allan variance of the residuals, from that model, is shown in Figure 20. Again, a 1/2 slope means that

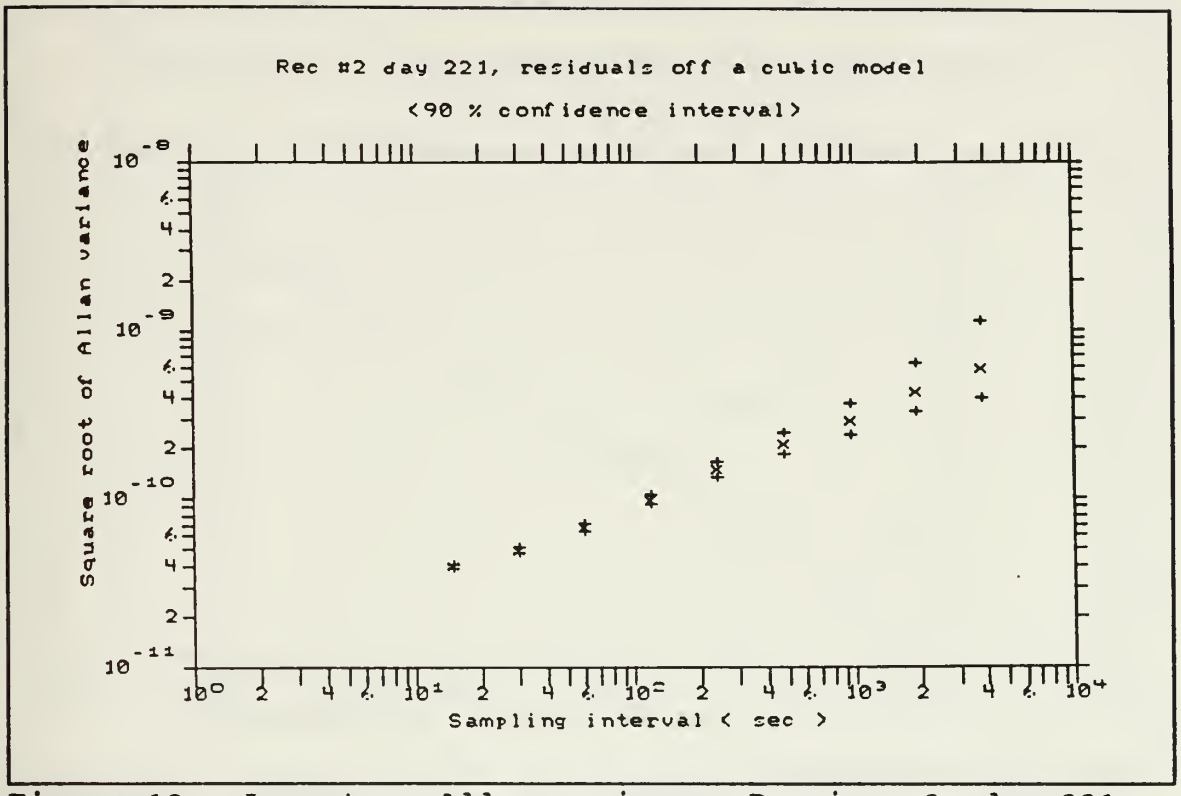

Figure 18.- Long term Allan variance. Receiver 2, day 221

the bulk of systematic effects has been removed. It shows good agreement with those in Figures 11 and 13.

The reader is warned about the validity of these results. A great deal of empiricism is underlying this last procedure. A more rigorous treatment of the temperature effects is needed. In particular, an environmental chamber is required to completely isolate the noise in the oscillator, from those induced by the temperature. In addition, analysis of longer data sets is desirable. Surveying observation sessions usually last for some three hours. The noise level at that sampling interval would be significant.

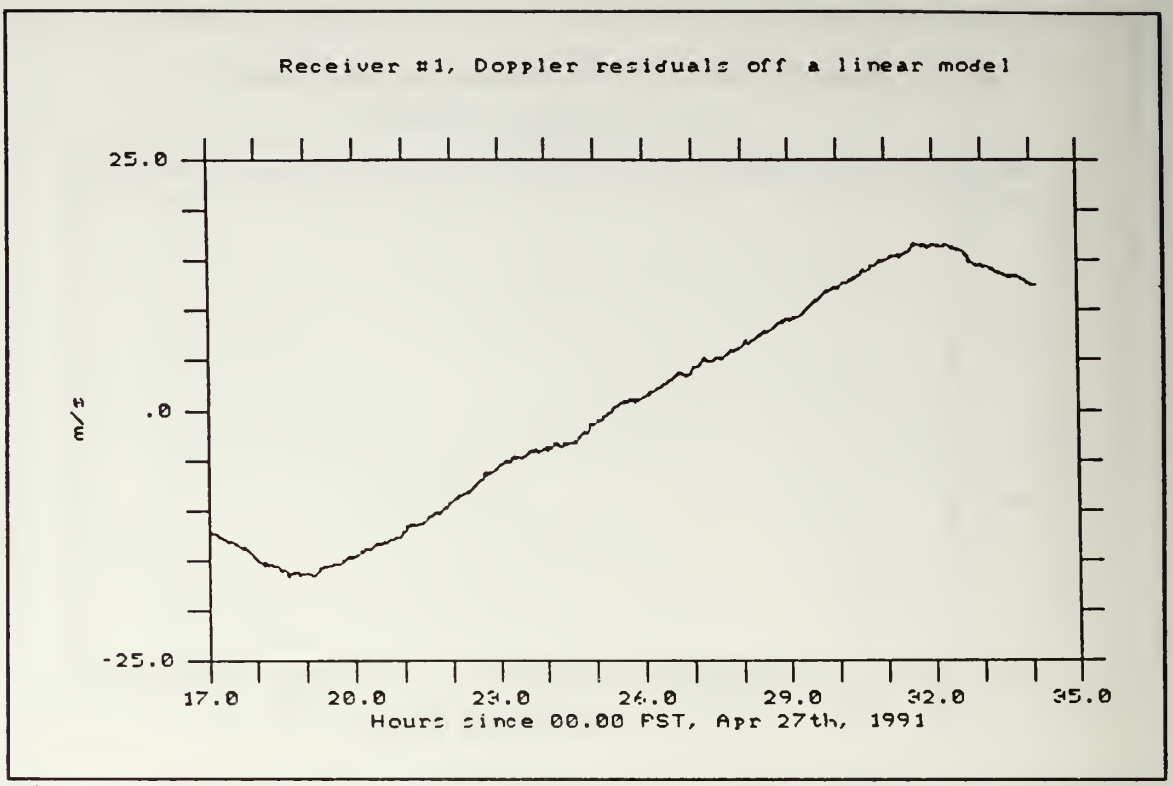

Figure 19.- Doppler residuals off a linear model. Receiver 1, day 117

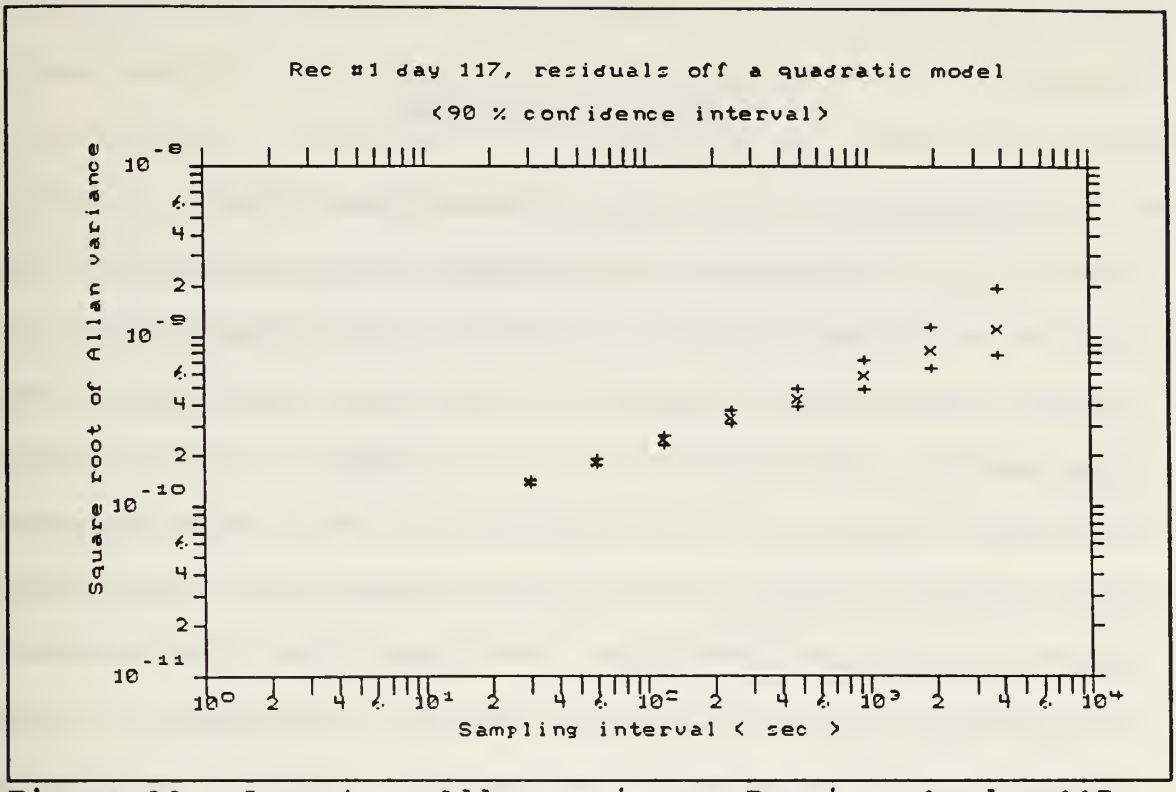

Figure 20.- Long term Allan variance. Receiver 1, day 117

VII. CONCLUSIONS

A new generation of inexpensive GPS receivers is emerging, which utilize temperature-compensated crystal oscillators. The use of an inexpensive clock implies higher rates of drift and sensitivity to environmental effects than customary in GPS applications. The question of the clock quality in one of these new receivers, the Magnavox 4200, has been addressed. The characteristics of the random noise in the measurements have been established for two particular receivers by comparison with the satellite clocks. The effect of the temperature on the oscillator frequency has been measured as well.

The receiver architecture is designed to minimize the noise in the pseudorange by means of a Doppler aided code tracking loop. Doppler frequency wipe off occurs before correlation. By integrating this Doppler frequency, a phase derived range is obtained. The time delay corresponding to this phase derived range is applied to the code replica generator. Thus, only the difference between pseudorange and phase range has to be tracked. This difference has a small variation, that can be tracked in a narrow bandwidth.

Measurements are simultaneously taken on six channels, at receiver time epochs. Clock and frequency offset are easily obtained as a part of the navigation solution, using an eight-

state Kalman filter. For a clock with such a high variability, those epochs can be offset several milliseconds from the GPS time after a few hours. In Time Recovery mode, the clock solution is used to dynamically correct the internal clock on a measurement by measurement basis.

Even temperature compensated crystal oscillators are very sensitive to temperature changes, at the levels of accuracy used in GPS. The effect of the temperature on the frequency offset was estimated. Experiments done on two receivers, showed that the transient regime lasted for two hours. Other tests showed that the thermal constant was about 20 $m/s/^0C$. Even in a mild environment, this may easily produce clock offsets of several miliseconds in just a few hours.

Temperature effects greatly complicated the analysis of the stochastic noise. A careful process was followed to isolate deterministic effects from the measurements. The stochastic noise in two receivers was obtained for sampling intervals up to 4000 sec. They show very similar characteristics. The Flicker floor is at about the measurement interval, one second. The Allan variance at one second sampling interval is on the order of $5x10^{-11}$. This implies inter-measurement random errors on the order of 1.5 cm due to clock offsets. The random walk frequency noise dominates at intervals of 4 seconds or more. At a 30 second sampling rate, the Allan variance is about 10^{-10}, implying about one meter of

clock induced random error in range. The trends imply that over a three hour observation session, the random component of the range, due to the clock noise, would grow to a few kilometers. The time tags would have random errors of tens of microseconds.

For high quality geodetic surveys, this has an important implication. The random noise can accumulate half a wavelength in just a few seconds, making integer cycles ambiguity resolution by clock modelling impossible. For all intended purposes the clock error must be solved for on a measurement by measurement basis. An observation session would require a continuous tracking of at least four satellites, with measurements every second.

LIST OF REFERENCES

1.- Clynch, J.R. and Coco, D.S., *Error Characteristics of High Quality Geodetic GPS Measurements: Clocks, Orbits and Propagation Effects*, Proceedings of the Fourth International Geodetic Symposium on Satellite Positioning, vol. 1, University of Texas at Austin, May 1986.

2.- Colquitt, E.S. and Anderle, R.J., *Effect of Oscillator Performance on Doppler Geodesy*, Proceedings of the Second International Geodetic Symposium on Satellite Doppler Positioning, vol. 1, University of Texas at Austin, January 1979.

3.- Wells, D., and others, *Guide to GPS Positioning*, Canadian GPS Associates, May 1987.

4.- Spielker, J.J., "GPS Signal Structure and Performance Characteristics", *Navigation*, vol. 1, The Institute of Navigation, Washington, D.C., 1980.

5.- Cannon, M.A., McLellan, J.F. and Schleppe, J.B., "High Accuracy Static GPS Surveys with Low Cost Receivers", paper submitted to *CSIM Journal*, June 1991.

6.- RTCM Special Committee no. 104, *RTCM Recommended Standards for Differential Navstar GPS Service*, Version 2.0, Radio Technical Commission for Maritime Services, Washington, D.C., January 1, 1990.

7.- Keegan, R., "The New Magnavox GPS Receiver Technology", paper presented at *ION GPS-90*, September 17-21, 1990.

8.- Magnavox Advanced Products and Systems Company, *MX4200 GPS Receiver and MX4200D Differential GPS Receiver Technical Reference Manual*, July 1990.

9.- Magnavox Field Service Bulletin, *MX4200 Firmware Release Announcement (B020, D020, N020)*, Magnavox Advanced Products and Systems Company, Marine and Survey Systems Division, April 1991.

10.- NBS Technical Note 616, *Frequency Standards and Clocks: a Tutorial Introduction*, by H. Hellwig, June 1977.

11- Press, W. H., Flannery, B. P., Teukolsky, S.A. and Vetterling, W.T., *Numerical Recipes. The Art of Scientific Computing (FORTRAN Version)*, Cambridge University Press, 1989.

12.- Stein, S.R., "Frequency and Time. Their Measurement and Characterization", *Precision Frequency Control*, vol.2, edited by E.A. Gerber and A. Ballato, Academic Press, New York, 1985.

13.- Allan, D. W., "Time and Frequency (Time Domain) Characterization, Estimation and Prediction of Precision Clocks and Oscillators", *IEEE Transactions on Ultrasonics, Ferroelectrics and Frequency Control*, v. UFFC 34, no. 6. November 1987.

14.- Barnes, J.A., "Data Analysis and confidence limits", presented to the *NIST Time and Frequency Seminar*, June 1989.

15.- Lesage, P., and Audoin, C., "Characterization of Frequency Stability: Uncertainity Due to the Finite Number of Measurements", *IEEE Trans. Instrum. Meas.*, v. IM-22, with corrections from *IEEE Trans. Instrum. Meas.*, v. IM-25, 1973.

16.- Yoshimura, K., "Characterization of Frequency Stability: Uncertainity due to the Autocorrelation of the Frequency Fluctuations", *IEEE Trans. Instrum. Meas.*, v. IM-27, 1-7.

17.- Hellwig, H., "Microwave time and frequency standards", *Radio Science*, v. 14, no. 4, July-August 1979

18.- NANU, *Notice Advisory to Navstar Users 121-91182*, USAF Space Command, Second Satellite Control Squadron, Falcon AFB, Colorado Springs, Co 80912-5000, July 1st, 1991.

APPENDIX A. AUTHOR'S SOFTWARE

1.- MXCKMO Computation of the coefficients of a polynomial, up to 4th degree, that models the receiver clock offset. Generates phase range residuals off that model. Linked to:

   a.- Subroutines in GAPP5 library: ASKSTA, ASKWTR, GETEPH, LDBTAB, RETRHO, SETGPS, STATL, STATR, STATXY, WGS84.

   b.- Subroutines in GEN5 library: WAIT.

   c.- Functions in GAPP5 library: ANLTRP, ELVANG.

   d.- Own subroutine: MXRDR1: Data interface to retrieve measurements and clock shift. Linked to:

      1.- Dr. Clynch's subroutines in MX42RTN library: IM4SET, M42SET, NXMX42.

      2.- Author's generated, following [Ref. 14:p. 31-39]: LUBKSD, LUDCMD, MPROVD.

2.- MXFXRS To fill in missing records in a residuals file; Halts process when a flagged residual is found.

3.- MERGE To add residuals files from different SV's to get a continuous sequence of residuals.

4.- MXALLV To compute point estimate the Allan variance of the residuals from a model.

5.- MXTRND To remove a clock offset model from a set of range measurements. Linked to:

a.- Subroutines in GAPP5 library: ASKSTA, ASKWTR, GETEPH, LDBTAB, RETRHO, SETGPS.

b.- Functions in GAPP5 library: ANLTRP, ELVANG.

c.- Own subroutine: MXRDR1.

6.- CONFIN To compute interval estimate Allan variance, from a point estimate file. Linked to the following subroutines, adapted from [Ref. 11:p. 160-165]: GSER, GAMMLN, GCF and functions GAMMP, GAMMQ.

APPENDIX B. ARL SOFTWARE

1.- Executable programs:

a.- DIFDAT2 To get differences across residuals.

b.- EPHSUM To get summary of an ephemeris file.

c.- GS2FIC To convert an ephemeris file in FIC format to ASCII format.

2.- Called subroutines.

a.- GAPP5 library:

1.- ASKSTA prompts for ground station input.

2.- ASKWTR prompts for metorological data.

3.- GETEPH fetches ephemeris table to retrieve the closest set.

4.- LDBTAB Loads array of ephemeris in a file.

5.- RETRHO computes slant range to the SV.

6.- SETGPS loads GPS parameters.

7.- STATL Initializes statistics array.

8.- STATR Inputs new value to statistics array.

9.- STATXY Get statistics from array of values.

10.- WGS84 Loads WGS 84 reference system parameters.

11.- Function ELVANG computes elevation angle of a SV.

12.- Function ANLTRP computes Hopfield tropospheric delay model.

APPENDIX C. DR. CLYNCH'S SOFTWARE

1.- Executable programs:

a.- GP: General Plot package, microcomputers version.

b.- MX2EPH: Extracts ephemeris from a data file and convert them into a FIC binary format.

c.- MXR package: data logger for the MX4200 receiver.

d.- MX42RTN library; contains:

1.- NXMX42 Reads raw data files, one record at a time, and loads values in arrays.

2.- MXCRK2 Decompresses block 2's and load values in arrays, as if done for block 1's.

3.- IM4SET Initialize data-solution-time block arrays.

4.- M42SET Gets in a single block all data, solution and time records belonging to the same epoch.

APPENDIX D. OMLS ADJUSTMENT

At a given epoch i the physical clock offset is first estimated by comparing measured pseudoranges with computed ranges. These observed-minus-computed ranges, scaled to time (ϵ), enter in an Ordinary Mean Least Squares Adjustment (OMLS). The mathematical model is:

$$\begin{aligned}\tau(t) &= a + b(t-t_0) + \frac{c}{2}(t-t_0)^2 + \frac{d}{6}(t-t_0)^3 \\ &= a + b\Delta t + \frac{c}{2}\Delta t^2 + \frac{d}{6}\Delta t^3\end{aligned} \tag{96}$$

i.e.,

$$\vec{\tau}(t) = H(\Delta t)\ \vec{x} \tag{97}$$

Here $\vec{x}$ is the column vector of the polynomial coefficients a, b, $c/2$, $d/6$, and

$$H(\Delta t) = [1 \quad \Delta t \quad \Delta t^2 \quad \Delta t^3] \tag{98}$$

is the design matrix. The elements Δt_i are the intervals between measurement and reference epoch, at epoch i, in GPS time.

The parameters are first set to 0, so at epoch i

$$\epsilon_i^0 = \frac{\rho_i - r_i}{c} \tag{99}$$

where ρ_i, r_i are the measured and true ranges to the SV.

After inversion

$$\vec{x}^1 = (H^T H)^{-1} H^T \vec{\epsilon}^0 \tag{100}$$

Given this first set of coefficients, a new clock offset can be computed for every measurement epoch. Those clock offsets are now subtracted from the previous OMC's, having

$$\epsilon_i^1 = \frac{\rho_i - r_i}{c} - \tau_i^0 \tag{101}$$

The process can be iterated, so

$$\Delta\vec{x}^1 = (H^T H)^{-1} H^T \vec{\epsilon}^1 \tag{102}$$

and the adjusted parameters after first iteration will be:

$$\vec{x}^1 = \vec{x}^0 + \Delta\vec{x}^1 \tag{103}$$

Subsequent iterations lead to better estimates of the parameters. Once the convergence criteria is met, after j iterations, the adjusted coefficients of the polynomial will be:

$$\vec{x}^{j} = \vec{x}^{j-1} + \Delta\vec{x}^{j} \qquad (104)$$

The whole process usually converges after four iterations.

INITIAL DISTRIBUTION LIST

1.	Defense Technical Information Center Cameron Station Alexandria, VA 22304	2
2.	Library, Code 52 Naval Postgraduate School Monterey, CA 93943-5000	2
3.	Chairman (Code OC/Co) Department of Oceanography Naval Postgraduate School Monterey, CA 93943-5000	1
4.	Dr. James R. Clynch (Code OC/Cl) Department of Oceanography Naval Postgraduate School Monterey, CA 93943-5000	3
5.	Dr. Jeffrey B. Knorr (Code EC/Ko) Department of Electrical and Computer Engineering Naval Postgraduate School Monterey, CA 93943-5000	1
6.	Excmo. Sr. CA Director Real Observatorio de Marina 11110 San Fernando (Naval). Cadiz, Spain	1
7.	Sr. C.N. Jefe Seccion de Guerra Acustica y Navegacion Division de Estrategia del E.M.A. Cuartel General de la Armada 28071 Madrid, Spain	1
8.	Sr. C.N. Comandante Director Instituto Hidrografico de la Marina 11071 Cadiz, Spain	1

9. Defense Mapping Agency System Center — 3
Attention:
Mr. R. Ziegler
Mr. S. Malys
Mr. M. Kumar
8613 Lee Highway
Fairfax, VA 22031-2138

10. Defense Mapping Agency Headquarters — 1
Attention: Mr. J. Slater
8613 Lee Highway
Fairfax, VA 22031-2138

11. Defense Mapping Agency H.T.C. — 2
Commander Geodetic Survey Group
Attention:
Mr. J. Rees
Mr. H. Heurman
P.O Box 9617
F.E. Warren AFB, WY 92005-6300

12. Magnavox Advanced Products Division — 4
Attention:
Mr. R. Hatch
Mr. R. Skeans
Mr. R. Keegan
Mr. B. Rodilitz
2829 Maricopa St.
Torrence, CA 90503

13. National Institute of Standards and Technology — 1
Attention: Mr. D. Allan
325 Broadway, Building 1
Boulder, CO 80303

14. Naval Surface Weapons Center - Dahlgren Laboratory — 3
Attention:
Mr. R. Hill (K 10)
Mr. A. Evans (K 10)
Mr. B. Herman (K 10)
Dahlgren, VA 22448

15. Navy Space Systems Activity — 1
Attention: CMDR J.R. McDermott (Code 80)
Los Angeles Air Force Station
P.O. Box 92960
Los Angeles, CA 90009-2960

16	Phillips Laboratory Attention: Mr. J. Klobuchar (LIS) Hanscon Air Force Base. MA 01731-5000	1
17	U.S. Naval Observatory Attention: Mr. B. Klepeziuski 34th and Massachusetts Ave. N.W. Washington D.C. 20392-5100	1
18	Steve Leiber and Associates Attention: Mr. Steve Leiber 610 W. Main St., Suite 107 League City, TX 77573	1
19	Dr. Stevens P. Tucker (OC/Tx) Department of Oceanography Naval Postgraduate School Monterey, CA 93943-5000	1
20	C.C. Manuel Pardo de Donlebun Seccion de Hidrografia Instituto Hidrografico de la Marina 11071 Cadiz, Spain	1

Thesis
P1515 Pardo
c.1 Chracterization of the clock in a new inexpensive GPS receiver.

DUDLEY KNOX LIBRARY
3 2768 00032013 9